

Integration of the 1,2,3-Triazole “Click” Motif as a Potent Signalling Element in Metal Ion Responsive Fluorescent Probes

Sandra Ast,^[a] Tobias Fischer,^[b] Holger Müller,^[a] Wulfhard Mickler,^[a]
Mathias Schwichtenberg,^[a] Knut Rurack,^{*,[b]} and Hans-Jürgen Holdt^{*,[a]}

Abstract: In a systematic approach we synthesized a new series of fluorescent probes incorporating donor–acceptor (D–A) substituted 1,2,3-triazoles as conjugative π -linkers between the alkali metal ion receptor *N*-phenylaza-[18]crown-6 and different fluorophoric groups with different electron-acceptor properties (4-naphthalimide, *meso*-phenyl-BODIPY and 9-anthracene) and investigated their performance in organic and aqueous environments (physiological conditions). In the charge-transfer (CT) type probes **1**, **2** and **7**, the fluorescence is almost completely quenched by intramolecular CT

(ICT) processes involving charge-separated states. In the presence of Na^+ and K^+ ICT is interrupted, which resulted in a lighting-up of the fluorescence in acetonitrile. Among the investigated fluoroionophores, compound **7**, which contains a 9-anthracenyl moiety as the electron-accepting fluorophore, is the only probe which retains light-up features in water and works as a highly K^+/Na^+ -selective probe under simulat-

ed physiological conditions. Virtually decoupled BODIPY-based **6** and photoinduced electron transfer (PET) type probes **3–5**, where the 10-substituted anthracen-9-yl fluorophores are connected to the 1,2,3-triazole through a methylene spacer, show strong ion-induced fluorescence enhancement in acetonitrile, but not under physiological conditions. Electrochemical studies and theoretical calculations were used to assess and support the underlying mechanisms for the new ICT and PET 1,2,3-triazole fluoroionophores.

Keywords: charge transfer · click chemistry · electron transfer · fluorescent probes · metal ions

Introduction

Fluorometric techniques are indispensable tools to assess the quantity of analytes at site, in situ or in ever smaller sample volumes in the laboratory and to image the topology of objects at nanometric dimensions.^[1–11] Despite the development of new types of powerful labels and probes such as fluorescent proteins or conjugated polymers,^[12,13] Förster (or as frequently termed: fluorescence) resonance energy transfer (FRET) ensembles or optical switch probes,^[14,15] semiconductor nanocrystals or up-converting nanoparticles,^[16,17] indicator dyes continue to be the most abundant form of fluorescent reporter employed. Accordingly, their development receives unquenched attention. Besides a number of non-

classical approaches proposed recently,^[18,19] the design strategies commonly follow three major routes: i) intramolecular charge-transfer (CT or ICT) active probes with a binding site integrated into a π -conjugated electron donor–acceptor-substituted fluorophore, ii) photoinduced electron transfer (PET) active probes with alkyl spacer-separated binding site and fluorescent group and iii) excimer probes with specific integration of binding site and polycyclic aromatic hydrocarbon fluorophores.^[20–22] However, a large number of such probes reported so far harbors several drawbacks such as the requirement of an organic (co-) solvent for operation of most ICT probes,^[23] the lack of spectral discrimination between bound and unbound form for PET probes^[29] and the restrictions in system design for excimer probes. The quest for potent yet straightforward design strategies thus remains highly topical.^[32,33]

Traditionally, one of the key areas of fluorescent probe development is the detection and tracking of metal ions in a large variety of environmental and biomedical samples and situations.^[34,35] Targets range from heavy metal ions through dia- and paramagnetic transition metal ions to alkaline-earth and alkali metal ions.^[36–40] The molecular toolbox comprises classical indicator dyes as well as aptamers,^[20–22,41] and techniques include conventional one-photon and spatially higher resolving two-photon excited fluorescence spectroscopies.^[42,43]

A continuing challenge in small-molecule probe design for metal ion analysis under physiological conditions is the

[a] S. Ast, H. Müller, Dr. W. Mickler, M. Schwichtenberg, Prof. Dr. H.-J. Holdt
Institut für Chemie, Anorganische Chemie, Universität Potsdam
Karl-Liebknecht Str. 24–25, 14467 Golm (Germany)
Fax: (+49) 331-977-5055
E-mail: holdt@uni-potsdam.de

[b] T. Fischer, Dr. K. Rurack
Fachbereich 1.9 Sensormaterialien
BAM Bundesanstalt für Materialforschung und -prüfung
Richard-Willstätter Str. 11, 12489 Berlin (Germany)
E-mail: knut.rurack@bam.de

Supporting information for this article is available on the WWW under <http://dx.doi.org/10.1002/chem.201201575>.

quest to obtain pronounced spectroscopic responses upon binding of monovalent “hard” metal ions,^[44] that is, non-aminophilic alkali metal ions with a comparatively low charge density such as Na⁺ and K⁺.^[20–22] Even under ideal conditions such as in (mixed) organic solvents, ICT probes commonly show only moderate shifts of a few tens of nanometres and fluorescence enhancement or quenching factors for PET probes are often around or below 30 in the presence of such analytes. Few examples of more efficient indication have been reported^[47–52] so that the search for alternative signalling strategies has received strong attention in the last decades.^[53]

For several years, we are particularly interested in integrating efficient signal transduction pathways in small probe molecules. For instance, we have succeeded in establishing the concept of “virtual decoupling” for the fluorescence light-up detection of notoriously quenching heavy and transition metal ions and weakly coordinating alkali metal ions^[47, 48, 54] and the tuning of the interplay of two intramolecular ICT and PET processes through guest binding for the amplified fluorescence detection of Pd^{II}.^[55, 56] However, one of the major challenges in conceiving and testing uncommon or interacting signalling pathways with various fluorophores such as for instance popular anthracene, boron–dipyrromethene

(BODIPY) or coumarin dyes often is synthetic realization. When screening the recent literature on fluorescent probe development, however, it seems that the versatility of the rather young yet extremely popular Cu^I-catalyzed azide–alkyne cycloaddition (CuAAC) or “click” chemistry which has been widely successfully used as a bioconjugation method,^[57] might offer more opportunities for system design.^[58] Since the first report on a fluorescent probe incorporating the typical “click” motif,^[59] a large number of examples utilizing different fluorophores—from coumarin and rhodamine through pyrene and anthracene to dansyl and naphthalimide—for a number of metal ions—mainly heavy and transition metal ions though—have been reported.^[60] However, in these ensembles the 1,2,3-triazol-1,4-diyl moiety has been basically used as a chelating site, either isolated from^[61–65] or conjugated to the chromophore,^[59, 66–68] or as a synthetic link in a traditional, decoupled PET type of architecture.^[69] All of these approaches thus do not lead to uncommon signalling pathways or behaviour, that is, they show the common features of fluorescence enhancement in the presence of closed-shell cations as for example, Zn²⁺^[62–64, 68] and quench-

ing in the presence of open-shell cations such as, Ni²⁺ and Cu²⁺^[64, 66, 69] or heavy metal ions as for example, Hg²⁺.^[65, 67] The latter is basically due to the fact that the 1,2,3-triazole unit is electronically not an ideal partner for ICT or PET processes. As Diederich’s group has shown recently, this situation changes when the triazole unit is coupled with strong electron donor and acceptor moieties.^[70] We thus strived to exploit this option more deeply in the context of functional dye design and report here on a series of fluorescent probes incorporating donor–acceptor- (D-A) substituted 1,2,3-triazoles as conjugative π -linkers between receptor and fluorophore units. The responsive donor unit is *N*-phenylaza-[18]crown-6 as a model receptor for K⁺ and popular fluorophores such as anthracene, naphthalimide and BODIPY comprise the acceptor moiety (Figure 1).^[71] *N*-Phenylaza-

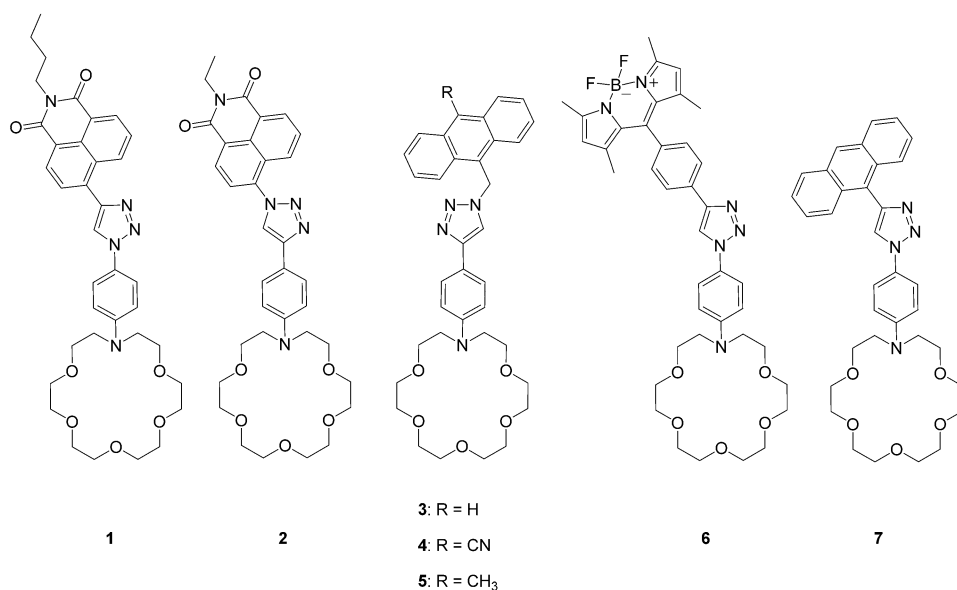


Figure 1. “Click”-type fluorescent probes investigated in this work.

[18]crown-6 and K⁺ (and Na⁺) were primarily chosen to assess the generality of the approach for a weakly coordinating analyte and to contrast it also with the majority of metal ion “click” probes that target transition metal ions because of the coordination chemistry of triazoles.^[73]

Our present aim is to assess the potential of providing the triazole unit in “click” probes with a decisive signalling function. Thus, it is essential to systematically study its performance in conventional ICT as well as PET architectures. Compounds **1** and **2** were thus prepared to elucidate whether the triazolyl–naphthalimide moiety with its favourable features^[62, 74, 75] can also be employed in a π -conjugated manner when coupled to an electron-rich receptor. Moreover, investigation of these two probes should provide more information about the role of the regioisomeric integration of the triazolyl moiety. Compounds **3–5** were synthesized as model PET probes, especially to be able to judge whether our ultimate approach of a CT/LE (locally excited)^[76] state-reversal

probe realized in **7** is superior to a conventional PET probe design with the same subunits. *meso*-Phenyl-BODIPY-incorporating **6** was attempted to get an idea whether the D–A triazole relay retains its performance in combination with a chromophore that absorbs in the visible spectral range instead of the UV as anthracene, naphthalimide and coumarin do. Finally, **7** was conceived as a first example of a probe containing a typical LE fluorophore such as anthracene in an all- π -conjugated architecture with the ICT-type triazole-aniline moiety, to allow for a unique interplay of LE and CT processes, potentially integrating features of the most popular signalling mechanisms.

Results and Discussion

With respect to the synthesis of the compounds, CuAAC of azido-functionalized *N*-phenylaza-[18]crown-6^[72,77,78] with *N*-(*n*-butyl)-4-ethynyl-1,8-naphthalimide,^[79] 4,4-difluoro-8-(4-ethynylphenyl)-1,3,5,7-tetramethyl-4-bora-3a,4a-diaza-*s*-indacene^[80–83] and 9-ethynyl-anthracene^[84] afforded **1**, **6** and **7**. The respective reaction of ethynyl-functionalized *N*-phenylaza-[18]crown-6^[72,85] with 6-azido-*N*-ethyl-1,8-naphthalimide,^[62] 9-azidomethyl-anthracene,^[86] 9-azidomethyl-10-cyanoanthracene,^[86,87] and 9-azidomethyl-10-methylanthracene^[86,88] yielded **2–5**. Details of the synthetic procedures and characterization are given in the Experimental Section and the Supporting Information, along with the synthetic details on the model compounds investigated here (Figure 2).

Spectroscopic properties of **1** and **2**:

For 4-(4-*R*-1*H*-1,2,3-triazol-1-yl)-anilines as well as 4-(1-*R*-1*H*-1,2,3-triazol-4-yl)-anilines (with *R*=substituent), Jarowski et al. have shown that the ICT process proceeds from the electron-rich aniline moiety to the electron-poorer triazole, carrying a further substituent either in the 4- or 1-position.^[70] On the other hand, for naphthalimide (NI) dyes it is well known that an ICT process can best be installed when a strong electron donor moiety such as a dimethylamino group is attached to the 4-position of the NI skeleton (as in **8**).^[89] As a consequence, we introduced the triazole-aniline unit in a vectorial fashion at the 4-position of the NI core, to arrive at composite

probes with two superimposed, directional ICT processes. Whereas **2** contains the more common 4-NI nitrogen atom, regioisomer **1** is connected through a carbon atom.

Table 1 lists the spectroscopic properties of both compounds in a highly polar model solvent such as acetonitrile. In comparison to for instance **8** (Figure 2), which absorbs and emits at 415 and 528 nm in acetonitrile and fluoresces with a reasonable quantum yield of 0.05,^[89,90] both **1** and **2** show dramatically reduced fluorescence quantum yields and hypsochromically shifted spectra, with a broad absorption band of considerable low intensity stretching out to about 500 nm in the case of **2** (see also Figure 3). The behaviour of **1** and **2** is also distinctly different from model compound **9**, carrying only the triazole unit without any additional donor group at the 4-position (Table 1).

To assess the photophysical mechanisms active in **1** and **2**, it is helpful to consider the electronic transitions and the respective states and molecular orbitals involved as obtained by quantum chemical calculations (Table 2, Figure 4). The typical naphthalimide-centred, oscillator-strong $S_1 \leftarrow S_0$ transition, involving HOMO and LUMO, has a certain CT character for 4-amino-substituted NI dyes and is for instance found at 385 nm in the gas phase for **8a** (imido *N*-ethyl analogue of **8**, Figure 2, Chart S1).^[92,94] If this 4-N atom is integrated in the weaker electron-donating triazole unit such as in **9**, the features of **8a** are largely preserved yet the CT

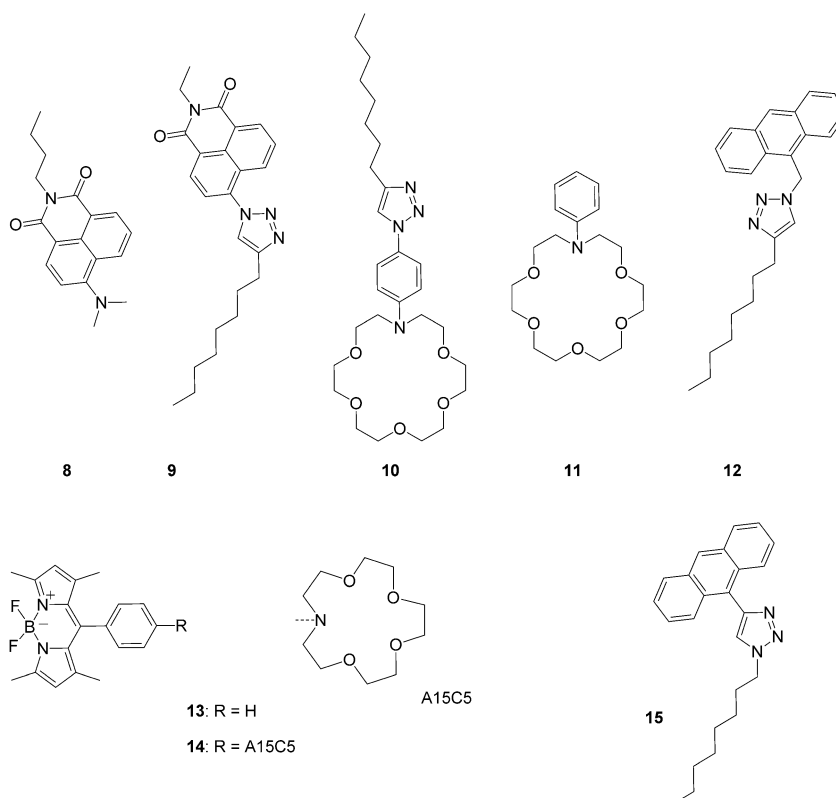


Figure 2. Model compounds experimentally investigated in this work; Theoretically investigated model compounds comprise **1a**, **2a** and **6a** as the *N,N*-dimethylamino analogues of **1**, **2** and **6**, **8a** as the imido *N*-ethyl analogue of **8** and **10a** as the *N,N*-dimethyl-3-ethyl analogue of **10b** and its regioisomer **10b** (see Chart S1, Table S5).

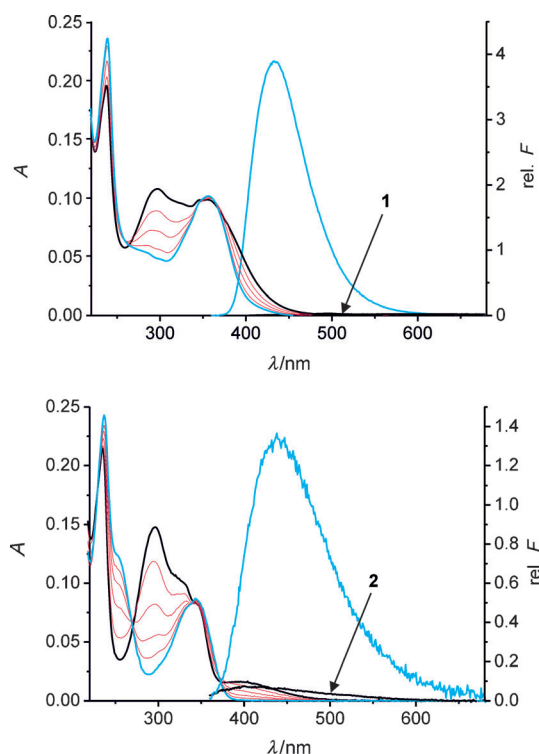


Figure 3. Absorption ($c_{\text{probe}} = 5 \times 10^{-5} \text{ M}$) and fluorescence spectra ($c_{\text{probe}} = 5 \times 10^{-6} \text{ M}$) of **1** (top, black lines) and **2** (bottom, black lines) in acetonitrile and corresponding titration spectra upon addition of Na^+ (red, selected steps between 0.25–13.0 mM; spectra of 1CNa^+ and 2CNa^+ as blue lines).

Table 1. Spectroscopic properties of **1**, **2**, their Na^+ and K^+ complexes as well as model compounds **8–10b** and Na^+ and K^+ complexes of **10a**.

Species	λ_{abs} [nm]	λ_{em} [nm]	ϕ_{f}	τ_{f} [ns]
1	239, 297, 347, 357	(500) ^[b]	10^{-4} ^[b]	< 0.01 ^[c]
1CNa⁺	239, 281, 360	434	0.10	3.38
1CK⁺	240, 281, 361,	444	6×10^{-4}	< 0.01 ^[c]
2	235, 296, 331, 345, 393	(470) ^[b]	10^{-4} ^[b]	< 0.01 ^[c]
2CNa⁺	237, 253, 336, 344	436	5×10^{-3}	0.24
2CK⁺	236 (263), 333, 344	(435) ^[b]	2×10^{-4}	0.01 ^[c]
8^[d]	415	528	0.05	0.8 (98) ^[e]
9	236, 334, 344	417	0.21	1.12
10	293	393	0.034	^[f]
10CNa⁺	273	^[f]	^[f]	^[f]
10CK⁺	276	393	0.048	^[f]

[a] In acetonitrile solution. [b] Too weak/low to be determined with acceptable accuracy with the instrument employed. [c] Within the temporal resolution of the instrument employed. Traces of a slow component are also found which are most likely due to traces of water/protons in the solvent used. [d] From ref. [89]. [e] Major component (98%) as given in ref. [89]. [f] Not determined.

character is weakened and the respective transition is shifted to shorter wavelengths (353 nm, Table 2). The corresponding NI-centred transitions in **1a** and **2a** (*N,N*-dimethylamino analogues of **1** and **2**, Figure 2, Chart S1) are, however, not the lowest transitions in these compounds, but only the second lowest $\text{S}_2 \leftarrow \text{S}_0$ transitions at about 358 and 350 nm. They involve HOMO–1 and LUMO in the case of **1a** and **2a**, with

Table 2. Calculated properties for the vertical excitation of the energy-minimized ground-state geometries of **1a** and **2a** and model compounds **8a** and **9** by TD-DFT (for calculation details, see Experimental Section).

	$\lambda_{\text{S}_n \leftarrow \text{S}_0}$ (n) [nm] ^[a]	f ^[b]	$\Delta\mu_{\text{S}_n \leftarrow \text{S}_0}$ (n) [D] ^[c]	Orbitals (coefficients) ^[d]
1a	422.0 (1)	0.130	40.1	HOMO–LUMO
	358.0 (2)	0.441	7.0	HOMO–1–LUMO
	340.2 (3)	0.003	–4.4	HOMO–2–LUMO
2a	570.4 (1)	0.079	39.9	HOMO–LUMO
	349.9 (2)	0.390	5.2	HOMO–1–LUMO (0.63) HOMO–4–LUMO (–0.15)
	343.2 (3)	0.026	0.4	HOMO–1–LUMO (0.14) HOMO–4–LUMO (0.67)
8a^[e]	385.5 (1)	0.215	9.2	HOMO–LUMO
	334.7 (2)	0.001	–0.7	HOMO–1–LUMO (0.55) HOMO–2–LUMO (0.41)
	306.1 (3)	0.002	–0.6	mixed (HOMO–3– LUMO)
9	352.8 (1)	0.348	6.0	HOMO–LUMO (0.64) HOMO–1–LUMO (0.10)
	344.1 (2)	0.001	5.4	HOMO–2–LUMO
	316.6 (3)	0.007	14.6	HOMO–LUMO (0.66) HOMO–2–LUMO (–0.13)

[a] Wavelength of the transition. [b] Oscillator strength of the transition. [c] Dipole moment difference between ground (μ_0) and respective excited (μ_n) state. [d] MOs involved in the transitions, mixed: more than four orbitals are involved. [e] The calculated structure of **8a** contains an ethyl instead of the *n*-butyl group at the imido nitrogen, which however has no significant influence on the findings.^[90] a minor contribution from HOMO–4–LUMO in the latter case. Thus, the typical NI $\text{S}_1 \leftarrow \text{S}_0$ transitions in **8a/8** and **9** become $\text{S}_2 \leftarrow \text{S}_0$ in **1a/1** and **2a/2**.

Table 2 and Figure 4 further reveal that the HOMO–LUMO transitions in the title dyes, which for both are equivalent to the $\text{S}_1 \leftarrow \text{S}_0$ transitions, lie at lower energies and have significantly smaller oscillator strengths. Moreover, these HOMO–LUMO transitions have a pronounced CT character with virtually complete charge localization in both molecular orbitals, also stressed by the large dipole moment differences between first ($\Delta\mu \sim 40 \text{ D}$) as well as second ($\Delta\mu \sim 6 \text{ D}$) excited and the ground state (Table 2). For **1a**, the $\text{S}_1 \leftarrow \text{S}_0$ transition is found at 422 nm and for **2a** even at 570 nm. Although the absolute positions as obtained by the calculations seem to be overestimated, they support the appearance of a red-shifted band of low intensity visible in the tailing of the long-wavelength band in **1** and the broad shoulder in **2**, stretching out to 500 nm. If one further considers that the electronic π -system is neither planar in **1a** nor in **2a** but significantly twisted by overall $\Sigma < (\theta_{\text{NT}} + \theta_{\text{TP}}) > 45^\circ$ (Table 3), the low intensity of the $\text{S}_1 \leftarrow \text{S}_0$ transition,

Table 3. Intramolecular torsion angles θ of the geometry-optimized ground state structures of **1a** and **2a**.^[a]

Species	θ_{NT} [°] ^[b]	θ_{TP} [°] ^[c]
1a	29.4	30.2
2a	45.4	0.9

[a] Naphthalimide plane defined by the 13 atoms of the NI core skeleton, triazole plane defined by the five ring atoms, phenyl plane defined by the six ring atoms. [b] Angle between NI and triazole planes. [c] Angle between triazole and phenyl planes.

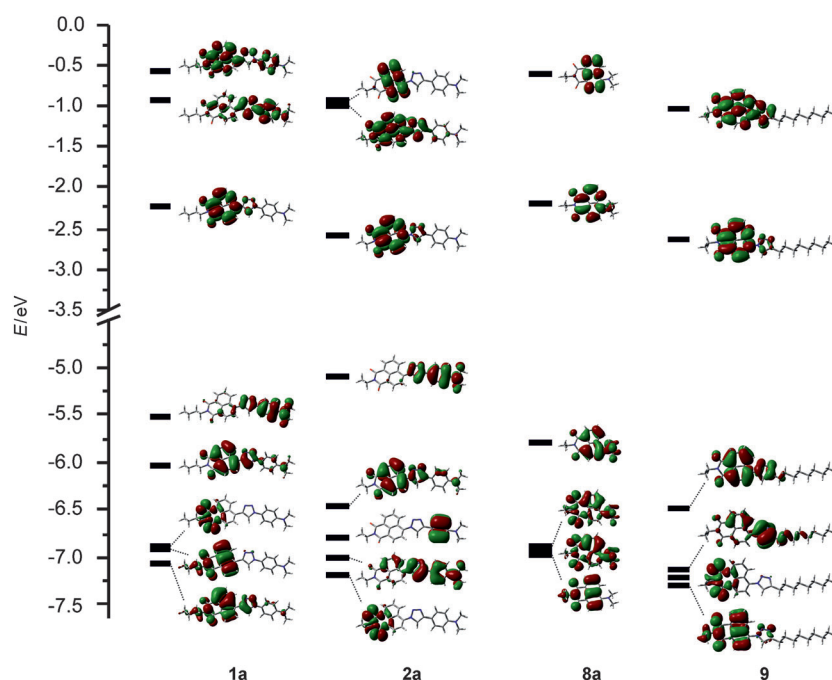


Figure 4. Frontier molecular orbitals HOMO–4, –3, –2, –1, HOMO, LUMO and LUMO+1, +2 of **1a** and **2a** and HOMO–3, –2, –1, HOMO, LUMO and LUMO+1 of **8a** and **9**.

which would be significantly broadened in a highly polar solvent such as acetonitrile compared to the gas phase calculations, also correlates well. Regarding the mismatch of the absolute position of that transition in the sense that TD-DFT calculations predict such charge-separated states to lie at rather low energies, our results are in line with similar findings by Diederich's group.^[70,95]

As is evident from Table 2, for both **1a** and **2a**, a series of weak to moderate transitions is found at $\lambda < 350$ nm, which are apparently responsible for the rich spectra in that region in Figure 3. Comparison of the absorption maxima of **1** with the relay-receptor model **10** (Figure 2) let us assign the intense band at about 295 nm to a transition located on the aniline–triazole fragment (Table 1), which is supported by the theoretical results listed in Table S5, that is, $S_5 \leftarrow S_0$ occurring at 295 nm and undergoing a moderate dipole moment change of $\Delta\mu = 8$ D for **1a**. This aniline–triazole-centred transition lies at slightly shorter wavelengths for **2a**, that is, 275.5 nm and possess a significantly higher oscillator strength (Table S5) which is in line with the ratio of the 295 to the 360 nm bands in **1** and **2** in Figure 3.

Although the oscillator strengths of the $S_1 \leftarrow S_0$ CT transition in **1a** and **2a** are reduced compared with the NI-centred $S_1 \leftarrow S_0$ transition with CT character in **8a** and **9**, this difference does not explain why the fluorescence quantum yields of **1** and **2** are more than two orders of magnitude lower than those of **8** and **9**. However, in contrast to **8a** and **9** for which the delocalization of HOMO and LUMO is largely identical, the strong charge localization and negligible orbital overlap of the frontier MOs in **1a** and **2a** is more reminiscent of strongly donor–acceptor substituted triaryl sys-

tems published in the literature.^[97,98] For such compounds, a twisting of the molecular subunits in the excited state can be a prominent non-radiative deactivation pathway especially in highly polar solvents, stabilizing charge separation and leading to low fluorescence quantum yields. We thus tentatively ascribe the pronounced quenching in the present case to such behaviour. In addition, closer inspection of the quantum chemical data provides a further hint. Whereas the singlet–triplet energy gap for the lowest or second-lowest excited states is 0.27 eV or higher in **8a** and **9**, it amounts to only 0.03 and 0.14 eV for **1a** and **2a**, potentially opening another efficient non-radiative deactivation pathway through intersystem crossing (Table S7). Summarizing the theoretical results it can

be said that in **1a/1** and **2a/2** a strong ICT process leading to pronounced charge separation between the molecular NI and triazole–aniline subunits and a very weakly emissive state masks the typical and usually highly emissive 4-amino naphthalimide-type CT process, entailing a strongly quenched fluorescence. The fact that **10** shows a moderate fluorescence (Table 1), yet **1** and **2** as well as the dyes reported in reference [70] are virtually non-emissive suggests that a D–A substitution pattern is mandatory to achieve quenching in a 1,2,3-triazole-based ICT architecture.

Electrochemical properties of 1 and 2: To facilitate the understanding of the processes at play, it is helpful to consider the redox properties of the title compounds. We thus investigated **1**, **2** and model compounds **9–11** by cyclic voltammetry in acetonitrile. Phenylazacrown **11** is irreversibly oxidized at +730 mV (Table 4). Whereas **2** shows a similar oxidation wave at +760 mV, only slightly anodically shifted compared with **11**, the corresponding potential is significantly shifted

Table 4. Selected redox potentials (peak, in mV) of **1**, **2**, **9–11** in the absence and presence of NaPF₆/KPF₆ in acetonitrile (for complete data, see Supporting Information, Table S9).^[a]

	1	2	9	10b	11
free	+900 _r –1260 _r	+760 _r –1140 _r	– –1150 _r	+860 _r –	+730 _{ir} –
+Na ⁺	+1020 _r –1270 _r	+950 _r –1050 _r	– –	+940 _r –	+770 _{ir} –
+K ⁺	+1020 _r –1260 _r	+960 _r –1050 _r	– –	+950 _r –	+760 _{ir} –

[a] Data against Fc/Fc⁺. Subscripts: r=reversible, ir=irreversible.

to +900 mV in **1**. However, when considering the respective oxidation at +860 mV in **10**, which contains the same formal phenylenediamine fragment as **1** does, it becomes evident that the regioisomer obtained from the *p*-azido-substituted phenylazacrown is more difficult to oxidize, presumably because of the electron-withdrawing effect of the N atom connecting the aniline moiety to the triazole ring. (Note that the sum of the Mulliken charges of this fragment obtained from the quantum chemical calculations amounts to 0.414 in **1a** yet only to 0.104 in **2a**.) In both **1** and **2**, the aniline-centred oxidation is reversible. Model compound **9**, representing the triazole–NI composite and here especially **2**, exhibits a reversible reduction at –1150 mV, which is very similar to the –1140 mV found for **2**. This is consistent with literature data on simple 1,8-naphthalimide derivatives, for instance, a reversible reduction at –1000 mV for 2-ethyl–NI and –1110 mV for 2-ethyl-6-methoxy–NI.^[99] A cathodic shift towards –1260 mV can be noted for **1** with the reversed triazole pattern. The other redox potentials which are not primarily important for the signaling process are given in the Supporting Information.

Response of **1 and **2** to Na⁺ and K⁺ under model conditions:** Following the design outlined above, that is, the masking of a highly emissive by a strong and non-emissive ICT process, the latter of which is generated especially by the bridgehead atom between electronic π -system and receptor moiety, the binding of a positively charged species such as a metal cation at this electron-rich aniline-N should redefine forces in the probe molecules, diminishing the quenching process. Indeed, as can be seen from Table 1 and Figure 3, addition of Na⁺ and K⁺ salts to an acetonitrile solution of **1** and **2** entails moderate changes in absorption, in particular the vanishing of the low-energy bands/tails of low intensity and the aniline–triazole-centred bands, and a large increase in fluorescence, especially for Na⁺. Comparison of for instance the spectral endpoint data in absorption of **2**Na⁺ and **2**K⁺ with those of **9**, the NI–triazole structural analogue of **2**, reveals a good agreement, suggesting that already the monovalent, non-aminophilic alkali metal ions can efficiently switch off the quenching ICT process in an aprotic organic solvent. The fluorescence of **2**Na⁺ and **2**K⁺ is still slightly red-shifted compared with **9**, which is most likely due to the fact that in such ICT probes the coordinative bond is weakened in the excited state, leading to electrostatic repulsion and partial de-coordination.^[100–102] An interesting conclusion that can be drawn from a comparison of the cation-induced effects on **1** and **2** is the fact that the spectroscopic response is much stronger for the regioisomer connected through the 4-C atom to the triazole than for the classic 4-N naphthalimide connection: **1**Na⁺ shows a much higher fluorescence enhancement than **2**Na⁺ and a 20-times brighter overall fluorescence (ϕ_f data in Table 1). Especially the impressive fluorescence enhancement factor of >100 for **1**Na⁺ is noteworthy, because such fluorescence amplification is rather uncommon for ICT-type probes. Regarding complex formation, the stoichiometries for the four

combinations all obey to a 1:1 model and the binding constants have been determined to $\log K(\mathbf{1} \subset \text{Na}^+) = 1.6$, $\log K(\mathbf{1} \subset \text{K}^+) = 2.7$, $\log K(\mathbf{2} \subset \text{Na}^+) = 2.8$ and $\log K(\mathbf{2} \subset \text{K}^+) = 3.2$. For example, $\log K(\mathbf{10} \subset \text{K}^+) = 3.2$. The finding that K⁺ forms stronger complexes than Na⁺ agrees well with the fact that [18]crown-6 better accommodates the larger K⁺ ion.^[103,104] Furthermore, the difference seen between the complexation constants of **1** and **2** also correlates well with the sum of the charges on the dimethylamino group as calculated for the dimethylamino analogues **1a** and **2a**, –0.135 and –0.148, such a correlation being a general design aid for ICT probes.^[94]

Assessing the ion response in acetonitrile by cyclic voltammetry results in an anodic shift of about 120 mV (for **1**) and about 200 mV (for **2**) of the oxidation of the receptor moiety for both Na⁺ and K⁺ (Table 4). The aniline-centred oxidation also becomes reversible, showing the stabilization of the ligand in the complexed state which has been reported before in the literature.^[78] Again, **10** which is regioisomerically similar to **1** shows virtually identical shifts in the presence of Na⁺ and K⁺ (Table 4), while the ion-induced effect is smaller for unsubstituted **11**. The minor differences seen for Na⁺ and K⁺ and **1** and **2** reflect well the minor differences seen in the cation-induced absorption shifts (Table 1). If we now consider the following observations that for both **1** and **2**, i) Na⁺ and K⁺ influence the electronic structure in the ground state to a comparable degree (absorption spectral and redox shifts), ii) Na⁺ leads to a much more pronounced fluorescence enhancement and iii) K⁺ forms the stronger ground-state complexes, it seems reasonable to assume that K⁺ is more tightly bound through the oxygen donor atoms of the crown, facilitating additionally a more efficient excited-state de-coordination from the crown's nitrogen atom.

Response of **1 and **2** to Na⁺ and K⁺ under simulated physiological conditions:** For a fluorescent probe that shows promising behaviour in model environments, the move to media for realistic analytical applications such as simulated physiological conditions (aqueous solution, buffered at pH 7.2 with 10 mM Tris and ≥ 1500 mM choline chloride for maintaining constant ionic strength) is usually the crucial step. Although **1** and **2** are only weakly soluble under such conditions, absorption measurements reveal that the CT transitions are significantly shifted. **1** shows now a broad band at about 440 nm while the weak band at 408 nm seen for **2** in acetonitrile is now still reduced in intensity with its maximum not being reliably detectable anymore (Figure 5). The fluorescence band of both compounds is also strongly shifted, to about 530 for **2** and 586 nm for **1**, which is in line with general findings on the fluorescence behavior of 4-donor-substituted NI dyes in water.^[105,106] In the case of **2**, the fluorescence is still very weak, hampering any more reliable determination of the fluorescence data. Interaction of the protic solvent with the aniline's nitrogen atom, which is expected to take place in this environment, is presumably not strong enough to lead to a significant increase in fluores-

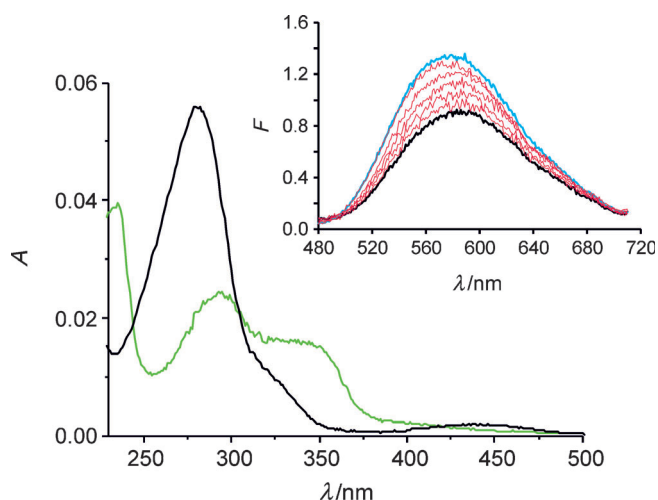


Figure 5. Absorption ($c_{\text{probe}} = 1 \times 10^{-5} \text{ M}$) spectra of **1** (black) and **2** (green) under physiological conditions (inset: corresponding titration spectra for **1** upon addition of K^+ (red, 5–160 mM; spectra of **1** and 1CK^+ as black and blue lines).

cence quantum yield. On the other hand, for **1**, the fluorescence quantum yield is slightly increased to $\phi_f = 2 \times 10^{-3}$. Addition of Na^+ and K^+ at concentrations between 5 and 160 mM, which represents the relevant physiological concentration range for these cations and especially for K^+ ,^[30,31] leads to negligible effects in the case of **2** and to a 1.4- and 1.5-fold fluorescence enhancement for Na^+ and K^+ and **1** (Figure 5). Although this enhancement is analytically not very exploitable, it shows that the design concept is rather powerful. Regioisomeric attachment of a triazole–aniline receptor unit through the triazole C4 atom to the acceptor of an ICT probe, like in **1**, thus seems to yield more powerful reporter molecules also in a realistic environment like we have observed in the case of a coumarin chromophore.^[72]

Spectroscopic properties of 3–5: The installation of a second, parallel ICT process by introduction of a “click” element has proven to be rather beneficial for creating a pronounced fluorescence enhancement for ICT-type probes. Compounds **3–5** were prepared to obtain further information in how far the donor-substituted 1,2,3-triazole unit is also a potent partner in a typical PET probe architecture.

The absorption spectrum of **3** shows the typical anthracene bands at 348, 367 and 387 nm, the strong anthracene band at 254 nm and a broad, intense band at 290 nm in acetonitrile (Figure 6). In addition, a weak anthracene-like fluorescence band is found. The features of **4** and **5** are rather similar, the slight spectral shifts being related to the influence of the substituent at the 10-position of the anthryl moiety (Table 5). Such features are typical for PET probe architectures consisting of anthracene, a methylene bridge and a substituted aniline receptor.^[107–109] For such compounds, quenching is commonly due to an electron transfer (ET) from the HOMO, which is localized entirely on the electron-rich aniline fragment, to the excited anthracene, on which fragment commonly HOMO–1 and LUMO are local-

Table 5. Spectroscopic properties of **3–5**, their Na^+ and K^+ complexes, and model compound **12**.^[a]

Species	λ_{abs} [nm]	λ_{em} [nm]	ϕ_f	τ_f [ns]
3	254, 292, 333, 349, 367, 387	391, 413, 438, 465	0.005	0.09 ^[d]
3CNa^+	254, 333, 349, 367, 387	391, 413, 438, 465	74 ^[e]	5.77
3CK^+	^[b]	^[b]	16 ^[e]	2.47
4	257, 292, 352, 369, 386, 408	419, 431 (468)	0.002	0.09 ^[d]
4CNa^+	257, 352, 369, 386, 408	418, 444, 468	365 ^[e]	10.61
4CK^+	^[b]	^[b]	2.5 ^[e]	0.1 ^[d]
5	259, 292, 339, 357, 376, 397	403, 427, 448	0.004	0.05 ^[d]
5CNa^+	258, 339, 357, 376, 397	403, 427, 448	120 ^[e]	8.45
5CK^+	^[b]	^[b]	35 ^[e]	4.07
12	254, 333, 348, 366, 386	390, 413, 437, 464	0.29	4.91

[a] In acetonitrile solution, $c_1 = 5 \times 10^{-6} \text{ M}$. [b] The spectral features of XCK^+ are virtually identical to XCNa^+ , $\text{X} = \mathbf{3}, \mathbf{4}$ or **5**. [c] Fluorescence enhancement with respect to unbound probe. [d] Traces of a slow component are also found which are most likely due to traces of water/protons in the solvent used. [e] Not determined.

ized.^[110] Reduction of the electron density at the aniline-N through protonation or complexation then revives emission. The situation is similar in **3–5**. If one compares the data of **10** and **12** in Tables 1 and 5 with those of **3**, it is evident that the absorption spectrum of **3** is a linear combination of aniline–triazole- and anthracene-centred transitions. (The transition that is localized exclusively on the isolated triazole fragment in **12** presumably lies outside of the wavelength range considered here, that is, at higher energies. Moreover, regardless of regioisomeric substitution pattern, the aniline–triazole-centred transition is found at about 300 nm, see [70].) The quenching process is also obvious if one takes a look at the MOs of **3**, which are exemplarily shown in Figure S2, Supporting Information. Anthracene-centred excitation predominantly involves HOMO–1 and LUMO, and facilitates ET from the triazole–aniline-localized HOMO (Tables S6, S7).

Electrochemical properties of 3–5: Further support for the mechanisms involved is provided by an electrochemical investigation of the PET-type probes, together with a series of model compounds. The oxidation at about +730 mV given for **11** in Table 4 agrees well with the oxidation of the respective fragments in **3–5** (Table 6). Although not π -conjugated, it can be noted that the nature of the substituent attached to the anthracene at the 10-position has an influence on the stability of the free probe as well as on the stability of the complexes, because only the aniline-centred oxidations in **4**, **5** and 4CK^+ are reversible. The redox potentials obtained for the anthracene moieties are in agreement with redox potentials of substituted anthracenes from the literature. The lowest reduction potentials at about –2000 mV in **3**, **5** and **12** and –1500 mV in **4** are most likely anthracene-based,^[111] whereas the second, more positive reduction at

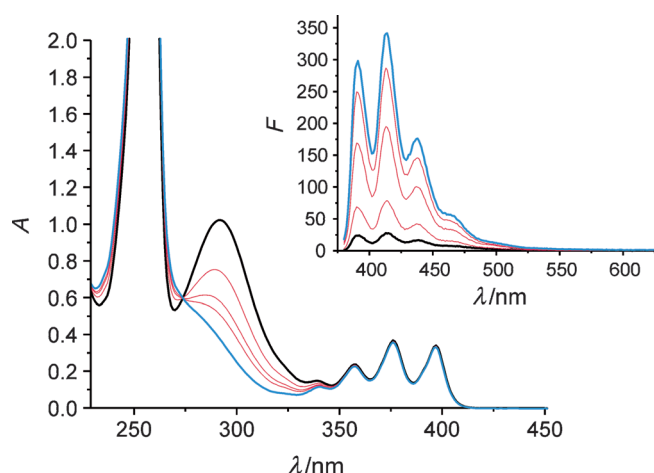


Figure 6. Absorption ($c_3=5\times 10^{-5}$ M) and fluorescence spectra (inset, $c_3=5\times 10^{-6}$ M) of **5** and **3** in acetonitrile and corresponding titration spectra upon addition of K^+ (red, 0.25–2.83 mM; spectra of $5C^+K^+$ in absorption and $3C^+K^+$ in fluorescence as blue lines).

Table 6. Selected redox potentials (peak potentials, in mV) of (**3–5**) and **12** in the absence and presence of $NaPF_6/KPF_6$ in acetonitrile (for complete data, see Supporting Information, Table S10).^[a]

	3	4	5	12
free	+1360	+1660	+1280 _r	+1470 _r
	+720	+750 _r	+740 _r	–
	–1750	–1280	–1770	–1780
	–2030	–1500	–2030	–2040
+Na ⁺	+1360	+1690	+1270	–
	+890	+910	+940	–
+K ⁺	+1360	+1700	+1270	–
	+850	+850 _r	+880	–

[a] Data against Fc/Fc^+ . Subscript r denotes reversible reactions.

about –1760 mV for **3**, **5** and **12** and –1280 mV for **4** originates from the triazole unit; such a reduction wave is lacking in anthracene.^[111] Considering the oxidation of anthracene, it is found at about 200 mV more positive values in the ligands than in the analogous substituted anthracenes (see Table 6 and ref. [111]). For example, the reversible oxidation of 9,10-dimethylanthracene (+1070 mV) occurs at +1280 mV in **5**, with the reversibility of the potential being retained.^[112]

Combination of the spectroscopic and the electrochemical data allows calculation of the PET driving forces according to the Rehm–Weller equation^[113] and yields values of –0.50, –0.84 and –0.41 eV for **3**, **4** and **5**, respectively, reflecting well the distinctly stronger quenching and ion-induced revival of the fluorescence in **4** compared with **3** and **5**.

Response to Na⁺ and K⁺ under model conditions: As expected for PET probes of the present type, addition of Na^+ and K^+ to acetonitrile solutions of **3–5** leads to a disappearance of the triazole-aniline CT band at 290 nm and a revival of the typical anthracene emission (Figure 6), which is virtually identical for $3C^+Na^+/K^+$ and model compound **12**. The behaviour of the broad CT-type band at about 280 nm,

which shifts from 293 to about 275 nm for **10** upon binding to the alkali metal ions (Table 1), is well reflected by the spectral changes in that region displayed by **5** (Figure 6), where it is only seen as a shoulder on the low-energy side of the intense anthracene absorption band at 254 nm in $5C^+K^+$. The behaviour is similar for **3** and **4**. The binding constants for 1:1 complexation have been determined to $\log K(3C^+Na^+)=3.0$, $\log K(3C^+K^+)=3.15$, $\log K(4C^+Na^+)=2.74$, $\log K(4C^+K^+)=3.6$, $\log K(5C^+Na^+)=2.23$ and $\log K(5C^+K^+)=3.5$.

With regard to the electrochemical behaviour, in general, complexation with Na^+ or K^+ leads to a positive shift of the oxidation potential and is slightly more pronounced for the Na^+ complexes than for the K^+ complexes (Table 6).

Response of 3–5 to Na⁺ and K⁺ under simulated physiological conditions: Although the ion-induced effects in a model environment are favorable with respect to fluorescence switching (up to >350), upon moving to physiological conditions and assessing the sensing performance in the important concentration range for Na^+ and K^+ , **3–5** show only negligible changes, hence, are not qualified for signalling purposes. The PET probes are still largely quenched in the unbound state in water and complexation presumably does not modulate PET efficiently.

Spectroscopic properties of 6: Having established the validity of the “click” concept for a typical PET probe architecture, our interest was to elucidate the potential of the triazole-aniline unit for integration with a fluorophore that absorbs and emits in the commonly more preferred visible spectral range. For this purpose, we chose a boron-dipyrromethene (BODIPY) fluorophore, which is one of the most popular fluorophores today because of various beneficial properties.^[116,117] In addition, integration of potentially strongly quenching analyte-responsive units in a virtually decoupled manner^[118] through the *meso*-position as in **6** (Figure 1) has been shown by others and us to yield powerful metal ion probes.^[47,48,54,119] These facts together with synthetic feasibility and accessibility of the precursor compounds let us pursue the design realized in **6**. The quest here was to judge whether the architecture that proved most promising for the NI dyes also performs well with this fluorophore. Table 7 shows that **6** is distinctly quenched in ace-

Table 7. Spectroscopic properties of **6** its Na^+ and K^+ complexes as well as **13** and **14**.^[a]

Species	λ_{abs} [nm]	λ_{em} [nm]	ϕ_f	τ_f [ns]
6	248, 308, 498	508	0.06	0.58 ^[c]
$6C^+Na^+$	255, 498	508	5.0 ^[b]	2.83
$6C^+K^+$	255, 498	508	4.5 ^[b]	2.54
13 ^[d]	229, 497 ^[e]	505	0.60	3.17
14 ^[d]	229, 265, 496 ^[e]	505	2×10^{-4}	<0.01

[a] In acetonitrile solution. [b] Fluorescence enhancement with respect to unbound probe. [c] Traces of a slow component are also found which are most likely due to traces of water/protons in the solvent used. [d] From ref. [47]. [e] Several weak BODIPY-centred bands between 285 and 420 nm not listed; 265 nm = aniline band in **14**.

tonitrile compared to the highly fluorescent model dye **13** (Figure 2), yet it is still much better fluorescent than BODIPYs with a directly *meso*-fused phenyl-aza-crown unit like **14** (Table 7). Evaluation of the optical transitions and MO energetics of model analogue **6a** (*N,N*-dimethylamino analogue of **6**, Figure 2, Chart S1) as obtained by quantum chemical calculations revealed that HOMO and LUMO are both localized on the BODIPY fragment, unlike the different localizations of the frontier MOs in **1a**, **2a** and **3** (Figure S2, Tables S6, S7). The lowest transition, however, is again an oscillator-weak CT transition with a large dipole moment difference, involving HOMO-1 and LUMO. Moreover, whereas the CT state in **1a**, **2a** and **3** lies >0.50 eV at lower energies in the gas phase, this difference amounts to only 0.13 eV in **6a**. Thus, when attached to longer wavelength absorbing chromophores such as BODIPY, the quenching potential of the aniline-triazole unit seems to be gradually diminished.

Response to Na⁺ and K⁺: In acetonitrile model solutions, the response of **6** toward Na⁺ and K⁺ is as would be expected, that is, the fluorescence increases without significant spectral fluorescence shifts to be noticed.^[47,48] This is a well-known feature of such virtually decoupled probes. Likewise, only the CT band stemming from the triazole-aniline unit at about 295 nm, which overlaps entirely with higher transitions centred on the BODIPY fragment, is noticeably reduced while the typical BODIPY band at 498 nm is virtually unchanged (Figure S3). Since the fluorescence enhancement factors are much smaller than for other virtually decoupled BODIPY probes, for example, **14** it is not surprising that the move to physiological conditions does not entail any pronounced effects. In addition, **6** is only weakly soluble in water, shows signs of aggregation^[120] and a fluorescence with two maxima at about 535 and 640 nm which is still reduced compared with MeCN. Like **3–5**, the donor-substituted 1,2,3-triazole unit does not seem to qualify for a virtually decoupled probe architecture like in **6** under realistic conditions.

Spectroscopic properties of **7** and response to Na⁺ and K⁺ under model conditions:

So far, the introduction of the triazole-aniline-receptor moiety into a typical ICT, PET and virtually decoupled CT probe architecture revealed good to excellent performance under ideal conditions. Under more realistic conditions, however, only the performance of **1** was promising yet cation-induced effects were still not ideal to qualify the probe for actual applications in alkali metal ion indication. We thus strived to improve signalling by π -conju-

gating the unit responsible for the strongly quenching ICT process with an intrinsically highly emissive fluorophore such as anthracene, however, not in a virtually decoupled scenario such as in **6**, but in a π -conjugated manner as in **1**. Recently, anthracene-metal complex receptor π -conjugates were used for the detection of phosphate anions and non-covalent protein labelling in aqueous solution.^[121] Staying with the terminology of ICT and PET dyes, anthracene is a typical so-called locally excited or LE fluorophore, that is, a fluorophore for which the MOs involved in the self-centred transitions are distributed over the entire molecular fragment and dipole moment changes are usually small with $\Delta\mu \leq \pm 1$ D. The UV/Vis absorption spectrum of **7** in Figure 7

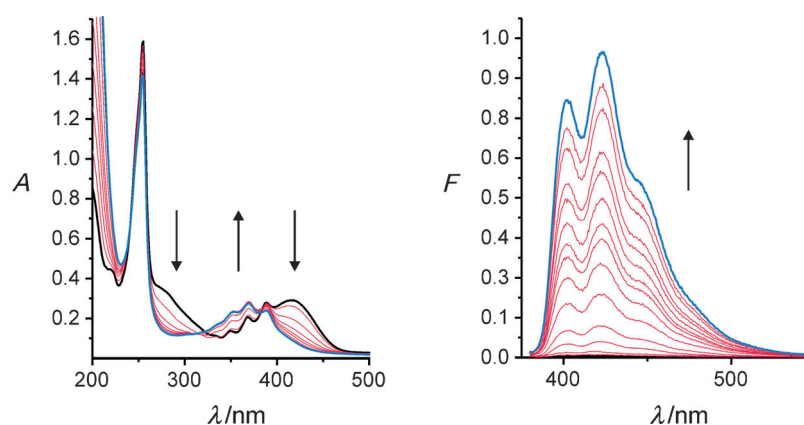


Figure 7. Absorption ($c_7=5 \times 10^{-5}$ M) and fluorescence spectra ($c_7=5 \times 10^{-6}$ M) of **7** (black lines) in acetonitrile and corresponding titration spectra upon addition of Na⁺ (red, 0.05–2.80 mM; spectra of **7CNa⁺** as blue lines). Arrows indicate changes upon cation addition.

reveals an intense band at 254 nm, a broad band with a maximum at 282 nm (after deconvolution) and a structured band of moderate intensity with maxima at 349, 368, and 387 nm that partly overlaps with a broader band of comparable intensity centred at 418 nm. The fluorescence of **7** shows two broad bands of low intensity, the integral fluorescence quantum yield ϕ_f amounting to 0.005 (Table 8, Fig-

Table 8. Spectroscopic properties of **7** and its Na⁺ and K⁺ complexes.^[a]

Species	λ_{abs} [nm]	λ_{em} [nm]	ϕ_f
7	254, 282, 349, 368, 387, 418	415, 539 ^[b]	0.005
7CNa⁺	254, 352, 369, 388	402, 423, 446	125 ^[c]
7CK⁺	254, 350, 369, 388, 414	402, 420, 445	13 ^[c]
15	254, 332, 348, 365, 385	403, 422	0.45

[a] In acetonitrile, $c_7=5 \times 10^{-6}$ M. [b] For spectrum, see Figure S4. [c] Fluorescence enhancement with respect to unbound probe.

ure S4). Such unstructured dual bands of reduced intensity are well-known for donor-substituted anthracenes, the blue-shifted band representing the residual LE fluorescence and the red-shifted band stemming from a weakly emissive CT state.^[122]

Before we attempt an assignment of the absorption bands to illustrate design, it is helpful to inspect the spectroscopic

changes induced by the complexation of alkali metal ions. As is evident from Figure 7, only the intense band at 254 nm and the structured bands in the 350–400 nm region remain unchanged upon addition of a metal ion in MeCN. The broad bands at 418 and 282 nm are significantly diminished and blue-shifted. The fluorescence titration spectra indicate that the emission of **7** is strongly enhanced. The band at 539 nm vanishes and the band shape of the spectrum of **7**C^{M+} is reminiscent of the structured anthracene emission. Moreover, the fluorescence enhancement is larger for Na⁺ (125-fold) compared with K⁺ (13-fold). In contrast, the complex stability constant is higher for K⁺ (log*K* = 3.0 vs log*K* = 2.6 for **7**CNa⁺). The latter behaviour can be rationalized in terms of the better fit-in-size of K⁺ into the 18-membered macrocycle^[103,104] and the stronger enhancement induced by Na⁺ is presumably due to the higher charge density and stronger ion–dipole interaction of this ion with the nitrogen bridgehead atom, especially in a solvent like acetonitrile that does not coordinate strongly with alkali metal ions (see also discussion for **1** and **2** above). Both cation-induced changes, however, suggest that the bands at 282 and 418 nm are typical CT bands the intensity of which is strongly reduced upon engagement of the nitrogen atom of the *N*-phenylaza-[18]crown-6 in complexation.

The unperturbed bands at 254 nm and 355–395 nm, together with the characteristic fluorescence spectrum, can thus be ascribed to the typical anthracene-localized transitions. These findings stress the previously outlined considerations that the anthracene fluorophore is the LE partner.

Signalling process in 7: To theoretically underpin the signalling mechanism, quantum chemical calculations were also performed for **7**. The optimized geometry of **7** reveals that the phenyl and triazole rings are twisted by 29.7° and the triazole and anthryl moieties by 58.5°.^[123] Figure 8 collects the frontier and next closest molecular orbitals (MOs) as derived from TD-DFT calculations. The corresponding data of the six lowest transitions are included in Table 9. For the isolated molecule in the gas phase, excitation to S₁ is dominat-

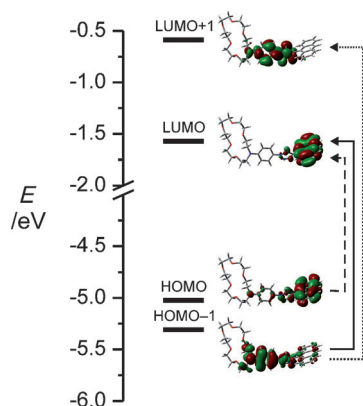


Figure 8. Frontier molecular orbitals of geometry-optimized **7**. Arrows denote major transitions between MOs mainly responsible for the S₁ (dashed), S₂ (solid) and S₆ (dotted) transition in the gas phase (for additional MOs, see Figure S5).

Table 9. Calculated properties of the six lowest vertical transitions of the optimized ground-state geometry of **7** by TD-DFT (for additional data, see Table S8).

S _n	λ _{S_n←S₀} (nm)	f ^[b]	Δμ _{S_n←S₀} [D] ^[c]	Orbitals (coefficients) ^[d]
S ₁	396.8	0.181	+3.4	HOMO–LUMO (0.64) HOMO–2–LUMO+3 (–0.11)
S ₂	367.4	0.001	+34.9	HOMO–1–LUMO (0.70)
S ₃	322.2	0.002	–1.3	6 mixed (mainly A)
S ₄	315.2	0.033	+12.8	6 mixed (incl. HOMO–LUMO+1)
S ₅	288.8	0.157	–1.0	6 mixed (mainly AT)
S ₆	288.4	0.493	+6.7	6 mixed (mainly AT)

[a] Wavelength of the transition. [b] Oscillator strength of the transition. [c] Dipole moment difference between ground (μ₀) and respective excited (μ_n) state. [d] MOs involved in the transitions. 6 mixed=six different MOs involved in mixed transition; mainly A/AT=mainly localized on anthracene/aniline-triazole fragment.

ed by the HOMO–LUMO transition with some admixture of a HOMO–2–LUMO+3 transition, all MOs being mainly localized on the anthracene moiety; oscillator strength *f* and dipole moment change Δμ are moderate to weak. According to Figure 8 and Table 9, the next lowest HOMO–1–LUMO transition shows all characteristics of a strong CT process with significant charge separation between two twisted fragments, that is, a large Δμ = 35 D and a low *f* = 0.001. The two next higher transitions are mixed transitions, largely involving MOs localized on the anthracene fragment with some CT character (anthracene to triazole–aniline) for S₄. S₅←S₀ and in particular S₆←S₀ with moderate to high *f* are also mixed transitions, now with a certain CT character within the triazole–aniline fragment.^[124] With respect to the absorption spectra in Figure 7, the transitions to S₆ (and S₅) are attributed to the band at 282 nm, the CT in the aniline–triazole fragment, and the fourth to first lowest transitions, except for S₂, to the typical anthracene-like and other weak bands at 300–400 nm. The S₂ transition finally is assigned to the unstructured absorption band at 418 nm. The discrepancy between theory (in the gas phase) and experiment (in acetonitrile) especially for the latter is evident when considering the stabilization that such a highly dipolar state experiences in a polar solvent such as acetonitrile. The large dipole moment difference presumably will lead to a state reversal and the HOMO–1–LUMO transition with a strong CT character will become the lowest transition, whereas the former S₁ will become S₂.

Having established the photophysics in free **7**, the processes happening upon complexation are obvious. Interaction of the cation with the crown ether nitrogen atom influences the electron donating character of the triazole–aniline fragment, resulting in a diminution of all CT bands accompanied by a strong, up to 125-fold enhancement of the anthracene or LE fluorescence. The design is thus based on a combination of a non-emissive CT process with a typical LE fluorophore in such a way that in the unbound state the lowest-lying transition is the CT and the second lowest the LE transition—hence, the free probe is virtually non-emissive—and

upon binding, the order of the states is reversed, switching the non-fluorescent CT for the strongly emissive LE state. Because the dye is entirely π -conjugated, the LE fluorophore acts at the same time as the acceptor in the CT process. In contrast to known CT/LE probes,^[125,126] this approach has the advantage that the LE state by design is highly emissive and that absorption spectral shifts are immanent to the system, which is for instance not the case for virtually decoupled “switch-on” probes.^[118,127] If one reconsiders now the picture for **1** and **2** given above, it is obvious that the analytically addressable process ($S_2 \leftarrow S_0$ in the gas phase and most likely $S_1 \leftarrow S_0$ in the condensed phase) is much better fine-tuned with regard to the highly emissive process in **7**.

Response to Na^+ and K^+ under physiological conditions:

Based on the favorable features reported for **7** in model media, the next step was to test the validity of the design concept under realistic conditions. Under simulated physiological conditions, the spectral features of **7** are not significantly changed with respect to acetonitrile—absorption bands at 255, 286, 351, 369, 388 and 423 nm and fluorescence at 427 nm—and the probe is also only weakly fluorescent ($\phi_f = 6 \times 10^{-3}$). Moreover, in the more competitive solvent, Na^+ is barely bound and only K^+ modulates the fluorescence to a sizeable degree, that is, leads to a 12-fold increase of the typical anthracene emission (Figure 9); for comparison: Na^+ only leads to a two-fold increase. If we further approach realistic conditions and add 2 mM of potentially competing Ca^{2+} and Mg^{2+} ions to the Tris-buffered and choline-containing medium and assess the relevant concentration range for K^+ sensing (0–160 mM K^+), the fluorescence increase is certainly lower but still amounts to a 3-fold increase for 160 mM K^+ . In addition to the analytical silence of Na^+ , it is important to note that 2 mM of Ca^{2+} and Mg^{2+} also do not interfere with K^+ indication. Although the crown unit chosen as model in our studies is not the ideal receptor for targeting alkali metal ions in water, the concept

seems very promising for the construction of potent fluorescent probes under realistic conditions.

Conclusion

The present report has shown how the different ways of incorporating a donor-substituted 1,2,3-triazole unit into conventional and newly conceived fluorescent probe architectures can lead to functional dye molecules that respond to metal ions with different combinations of absorption and fluorescence spectroscopic effects. Whereas the installation of two vectorial ICT processes in **1** and **2** led to absorption spectral shifts and a potent switching-on of the fluorescence in organic environments, aqueous solvents only gave a negligible response. Regioisomeric integration clearly seems to have an effect on the complex stability and fluorescence enhancement of these π -conjugated fluoroionophores.^[72] It should be noted that even for organic solvents, fluorescence light-up factors of >100 are very rarely found for ICT-type probes. The concept of integration in actually or virtually decoupled architectures gave varying light-up factors in acetonitrile but failed under physiological conditions, most likely because the photophysical processes are not directly coupled. However, especially for BODIPY dyes with their many attachment points for functional units, 3,5-integration might open up more promising possibilities. Newly designed **7**, however, showed favorable K^+ -sensing features under realistic conditions, even though it carries only a rather weakly binding receptor unit such as aza-[18]crown-6. The lighting-up mechanism proved to be especially interesting: Upon ion binding, the CT state is energetically shifted upwards and LE becomes S_1 , that is, state reversal occurs resulting in a fluorescence lighting-up. Moreover, the concept of using the donor-acceptor-substituted 1,2,3-triazole unit as relay elaborates our earlier approaches toward probes with more than one active photophysical process^[131] in the sense

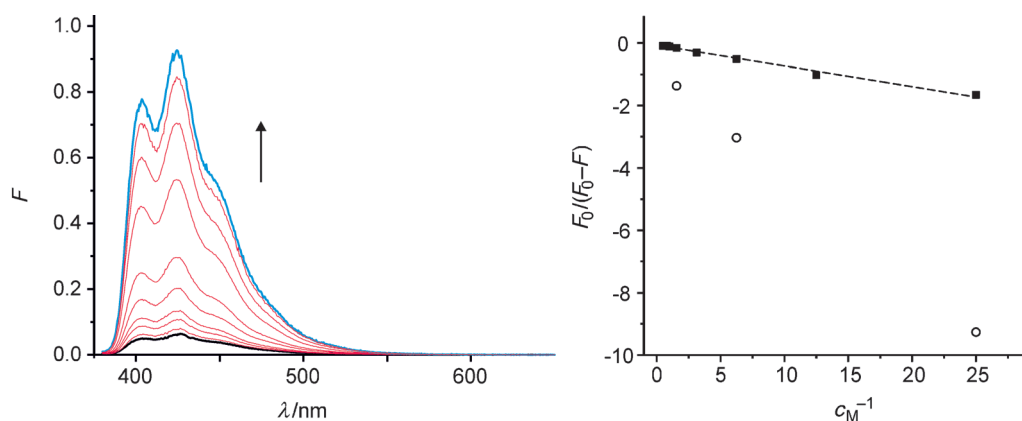


Figure 9. Left: Fluorescence spectrum of **7** (thick black line, $c_7 = 7 \times 10^{-6} \text{ M}$) in aqueous solution (buffered at pH 7.2, 10 mM Tris, $\geq 1500 \text{ mM}$ choline chloride for maintaining constant ionic strength) and corresponding titration spectra upon addition of K^+ (5–1500 mM; spectrum of **7** $\subset \text{K}^+$ as blue line). Right: Titration curve plotted according to a formalism for weak complexes $F_0/(F_0-F)$ vs. c_M^{-1} (F_0 = fluorescence intensity of unbound **7** at 435 nm and metal ion concentration $c_M = 0$, F = fluorescence intensity for steps of metal ion addition)^[130] for **7** and K^+ (black squares, $r^2 = 0.98$) and Na^+ (\circ) under similar conditions.

that **7** actually performs under realistic conditions. This important practical implication becomes possible by the choice of a suitable LE fluorophore that fluoresces strongly in water. Current research in our groups focuses on the integration of specific and more potent alkali and alkaline-earth metal ion receptors, to possibly improve the performance of established ion indication strategies, the application of the probes for K^+ , Na^+ and Ca^{2+} in biological samples and the further elucidation whether the combination of the aniline-triazole unit with other long wavelength-absorbing fluorophores also allows to construct powerful probes or whether an electronic modification of the relay unit might be necessary. In our view, especially the modularity of the approach is very appealing for approximating other potent fluorophore-receptor combinations.

Experimental Section

General methods and procedures: All commercially available chemicals were used without further purification. Solvents were distilled prior use. Air/water-sensitive reactions were performed in oven-dried glassware under an argon atmosphere. Column chromatography was performed with SiO_2 (Merck Silica Gel 60 (0.04–0.063 mesh)).

Optical spectroscopy: UV/Vis measurements were recorded on a Perkin-Elmer Lambda 950 spectrophotometer using 1 cm path length quartz cuvettes. Titrations of the compounds **1–7** ($c = 5 \times 10^{-5}$ M) were carried out in acetonitrile and recorded 5 min after the addition of 0.01 mL of volumetric standard solutions of respectively $NaPF_6$ or KPF_6 ($c = 5 \times 10^{-4}$ – 5×10^{-2} M) in acetonitrile. To ensure complete reaction towards the corresponding complex, titration was continued until no change in the UV/Vis absorption spectra was observed. Fluorescence titration spectra of the compounds **1–7** ($c = 5 \times 10^{-6}$ M) in acetonitrile were recorded 5 min after the addition of 0.02 mL of volumetric standard solution of $NaPF_6$ or KPF_6 ($c = 5 \times 10^{-5}$ – 5×10^{-2} M), respectively. Titration was continued until no change in fluorescence enhancement was observed. Fluorescence quantum yields were determined using a PL Quantum Yield measurement System C9920-2 from Hamamatsu and with the relative approach according to Parker and Rees^[136] on a Fluoromax 4 from Horiba Jobin-Yvon using quinine sulfate in 0.105 M perchloric acid ($\phi_f = 0.60$)^[137] or coumarin 153 in ethanol ($\phi_f = 0.54$)^[138] as the standard. Fluorescence lifetimes (τ) were determined with a FL920 fluorescence lifetime spectrometer (Edinburgh Instruments) with a Ti/Sa laser system in the frequency-doubled or tripled mode and with a unique customized laser impulse fluorometer with picosecond time resolution described in.^[52,139] The fluorescence decays were recorded with modular single photon timing units. The fluorescence lifetime profiles were analyzed with a PC using the software package Global Unlimited V2.2 (Laboratory for Fluorescence Dynamics, University of Illinois). The goodness of the fit of the single decays as judged by reduced chi-squared (χ_R^2) and the autocorrelation function $C(j)$ of the residuals was always below $\chi_R^2 < 1.2$.

Electrochemical measurements: Electrochemical data were determined with the electrochemical analyzer PGSTAT302N (Metrohm, Switzerland) and cell stand C3 (Bioanalytical Systems, USA) using a platinum disc working electrode (2 mm²), a platinum wire auxiliary electrode and an anhydrous Ag/Ag^+ -reference electrode.

Computational details: The optimization of the S_0 ground state geometries in the gas phase was performed with the density functional theory (DFT) method employing the hybrid functional B3LYP with a 6-31G-(d,p) basis set and energy-minimized as implemented in Gaussian 03.^[140]

Synthetic procedures: The preparation of *N*-phenylaza-[18]crown-6 ether (**11**),^[141] *N*-(4-ethynyl)phenylaza-[18]crown-6 ether (**16**),^[72,85] *N*-(4-azido)phenylaza-[18]crown-6 ether (**17**),^[72,77,78] 9-ethynylanthracene (**18**),^[84] 1-azidoctane (**19**),^[142,143] *N*-(*n*-butyl)-4-ethynyl-1,8-naphthalimide (**20**, Sup-

porting Information)^[79] and the 6-azido-*N*-ethyl-1,8-naphthalimide (**21**, Supporting Information)^[62,144] followed reported procedures and references therein.

9-Azidomethyl-anthracene (22): The synthesis followed the literature according to a modified procedure.^[86] A suspension of 9-chloromethylanthracene (1.00 g, 4.41 mmol) and sodium azide (0.43 g, 6.62 mmol, 1.5 equiv) in acetonitrile (30 mL) was refluxed for 5 h. After the reaction was complete (monitoring via DC) the reaction mixture was cooled to room temperature and the resulting solid was filtered off. The solution was concentrated in vacuo and the resulting yellow solid was purified by column chromatography (silica gel, *n*-hexane/ethyl acetate 3:1). Yield: 0.92 g (90%); m.p. 78–80 °C (lit.: 80–82 °C); ¹H NMR ($CDCl_3$, 500 MHz): $\delta = 8.52$ (s, 1H, H⁵), 8.29 (d, 2H, $J = 8.85$ Hz, H¹), 8.05 (d, 2H, $J = 8.40$ Hz, H⁴), 7.60 (m, 2H, H²), 7.52 (m, 2H, H³), 5.31 ppm (s, 2H, H⁶); ¹³C NMR ($CDCl_3$, 125 MHz): $\delta = 131.45, 130.79, 129.39, 129.09, 126.94, 125.87, 125.30, 123.31, 46.42$ ppm; FT-IR (KBr): $\nu = 2095$ (s), 1444 cm⁻¹ (m); MS (EI): m/z (%): 233 (100) [M^+].

9-Azidomethyl-10-cyanoanthracene (23):^[86,87] The synthesis followed the procedure for the preparation of **22** starting from 9-cyano-10-methylanthracene (**23b**, Supporting Information). The crude product was re-crystallized from $CH_2Cl_2/MeOH$ to give the product as yellow fluffy needles. Yield: 0.10 g, 39%; ¹H NMR ($CDCl_3$, 300 MHz): $\delta = 8.48$ (d, 2H, $J = 8.84$ Hz, H¹), 8.35 (d, 2H, $J = 8.13$ Hz, H⁴), 7.79–7.65 (m, 4H, H², H³), 5.33 ppm (s, 2H, H⁵); ¹³C NMR ($CDCl_3$, 75 MHz): $\delta = 133.04, 132.90, 129.94, 128.85, 127.84, 126.52, 124.48, 117.07, 108.08, 46.29$ ppm; FT-IR (KBr): $\nu = 2213$ (s), 2100 (s), 1444 cm⁻¹ (m); MS (+ESI): m/z : calcd for $C_{16}H_{11}N_4$: 259.10; found: 259.15.

9-Azidomethyl-10-methylanthracene (24): The synthesis followed the procedure for the preparation of **22** using 9-bromomethyl-10-methylanthracene (**24a**, Supporting Information).^[86,88] Yield: 0.98 g, 90%; ¹H NMR ($CDCl_3$, 300 MHz): $\delta = 8.39$ – 8.31 (m, 4H, H², H³), 7.63–7.53 (m, 4H, H³, H⁴), 5.34 (s, 2H, H¹), 3.14 ppm (s, 3H, H⁶); ¹³C NMR ($CDCl_3$, 75 MHz): $\delta = 132.91, 130.62, 130.03, 126.44, 125.74, 125.22, 124.29, 46.69, 14.64$ ppm; FT-IR (KBr): $\nu = 2214$ (s), 2114 (s), 1444 cm⁻¹ (m); MS (EI): m/z (%): 247 (100) [M^+].

4,4-Difluoro-8-(4-trimethylsilylethynylphenyl)-1,3,5,7-tetramethyl-4-bora-3a,4a-diaza-s-indacene (25b): The synthesis of 4-iodophenyl derivative **25a** (see also Supporting Information) followed the literature according to a modified procedure.^[80,81] The reaction towards (**25b**) followed a literature procedure for a similar reaction.^[85] [$PdCl_2(PPh_3)_2$] (91.2 mg, 0.13 mmol, 5.0 mol %), CuI (24.8 mg, 0.13 mmol, 5.0 mol %), TEA (770 μ L, 5.5 mmol, 2.2 equiv) and trimethylsilylacetylene (0.469 mL, 5.0 mmol, 2.0 equiv) were placed in a dry round-bottom flask before a solution of **25a** (740 mg, 2.5 mmol) in dry DMF (25 mL) was added. The reaction mixture was stirred for 5 h at 60 °C, then cooled to room temperature, diluted with H_2O and extracted with CH_2Cl_2 (100 mL). The combined organic phases were dried over $MgSO_4$, concentrated and the crude product was purified by column chromatography (silica gel, hexane/ethyl acetate 4:1 v/v), to give **25b** as a purple-red solid. Yield: 0.467 g, 67%; ¹H NMR ($CDCl_3$, 500 MHz): $\delta = 7.60$ (d, 2H, $J = 8.1$ Hz, H⁵), 7.23 (d, 2H, $J = 8.1$ Hz, H⁴), 5.98 (s, 2H, H²), 2.55 (s, 6H, H³), 1.39 (s, 6H, H¹), 0.28 ppm (s, 9H, H⁶); ¹³C NMR ($CDCl_3$, 125 MHz): $\delta = 155.89, 143.13, 140.88, 135.35, 132.86, 131.28, 128.21, 124.06, 121.49, 95.96, 29.84, 14.27, 1.17$ ppm; ¹⁹F NMR ($CDCl_3$, 300 MHz): $\delta = -146.7$ ppm (m, 2F); EI-MS: m/z (%): 420 (100) [M^+].

4,4-Difluoro-8-(4-ethynylphenyl)-1,3,5,7-tetramethyl-4-bora-3a,4a-diaza-s-indacene (25): The TMS-deprotection of **25b** (Supporting Information) was followed a literature procedure according to a similar reaction.^[82] Compound **25b** (100 mg, 0.239 mmol) was dissolved in a mixture of THF/MeOH (45 mL, 4:1 v/v) before a solution of tetrabutylammonium-fluoride (1 M in THF, 45 mL, 0.357 mmol, 1.5 equiv) was added. Stirring at room temperature was continued for 19 h. The reaction mixture was concentrated in vacuo and purified by column chromatography (silica gel, hexane/ethyl acetate 4:1 v/v) to give **25** as an orange solid (0.060 g, 73%). M.p. 245.5–250.1 °C; ¹H NMR ($CDCl_3$, 125 MHz): $\delta = 7.85$ (d, 2H, $J = 8.3$ Hz, H⁵), 7.05 (d, 2H, $J = 8.3$ Hz, H⁴), 5.99 (s, 2H, H²), 2.55 (s, 6H, H³), 2.17 (s, 1H, H⁶), 1.42 ppm (s, 6H, H¹); ¹³C NMR ($CDCl_3$, 500 MHz): $\delta = 156.88, 143.88, 141.05, 139.33, 135.56, 132.13, 130.95,$

122.43, 95.69, 15.67, 15.57 ppm; ^{19}F NMR (CDCl_3 , 300 MHz): $\delta = -146.6$ ppm (m, 2F); EI-MS: m/z (%): 348 (100) [M^+].

General CuAAC procedure: The reaction followed the literature.^[145] To the stirred suspension of Cu/C (0.1 equiv) in THF (3 mL) was added triethylamine (1.0 equiv) followed by the azide derivative (1.0 equiv) and the acetylene derivative (1.0 equiv). The reaction mixture was stirred at 60°C for 16 h after which an additional portion of the Cu/C (0.1 equiv) was added. It was heated for two days and cooled to room temperature before the Cu/C was filtered off through celite. Concentration of the solution gave the crude product which was purified by column chromatography.

2-Butyl-6-[1-[4-(1,4,7,10,13-pentaoxa-16-azacyclooctadecan-16-yl)phenyl]-1H-1,2,3-triazol-4-yl]-1H-benzo[de]isoquinoline-1,3(2H)-dione (1): Compounds **17** and **20** (Supporting Information) were reacted according to the general CuAAC procedure. The crude product was purified by column chromatography (silica gel, $\text{CHCl}_3/\text{MeOH}$ 98:2 v/v) to yield **1** as a yellow solid (0.086 g, 49%). M.p. 136.1–139.0°C; ^1H NMR (CDCl_3 , 600 MHz): $\delta = 9.1$ (dd, 1H, $J = 8.55, 1.05$ Hz, H^9), 8.63 (dd, 1H, $J = 7.02, 1.02$ Hz, H^7), 8.61 (d, 1H, $J = 8.55$ Hz, H^5), 8.26 (s, 1H, H^{10}), 7.99 (d, 1H, $J = 7.56$ Hz, H^6), 7.79 (dd, 1H, $J = 8.52, 7.26$ Hz, H^8), 7.61 (d, 2H, $J = 9.12$ Hz, H^{11}), 6.81 (d, 2H, $J = 9.12$ Hz, H^{12}), 4.18 (t, 2H, $J = 7.62$ Hz, H^4), 3.74–3.64 (m, 24H, H^{13-18}), 1.76–1.69 (m, 2H, H^3), 1.45 (sx, 2H, $J = 7.62$ Hz, H^2), 0.98 ppm (t, 3H, $J = 7.38$ Hz, H^1); ^{13}C NMR (CDCl_3 , 150 MHz): $\delta = 164.34, 164.06, 148.68, 146.15, 145.66, 134.32, 132.92, 131.52, 130.81, 129.40, 128.95, 127.48, 127.35, 125.96, 122.94, 122.56, 121.52, 111.99, 70.98-70.82, 68.8, 68.60, 51.59, 40.41, 30.32, 20.52, 13.99$ ppm; HRMS (^+ESI): m/z : calcd for $\text{C}_{36}\text{H}_{44}\text{N}_5\text{O}_7$: 658.3242; found: 658.3220.

2-Ethyl-6-[4-[4-(1,4,7,10,13-pentaoxa-16-azacyclooctadecan-16-yl)phenyl]-1H-1,2,3-triazol-1-yl]-1H-benzo[de]isoquinoline-1,3(2H)-dione (2): Compounds **16** and **21** (Supporting Information) were reacted according to the general CuAAC procedure. The crude product was purified by column chromatography (silica gel, $\text{CHCl}_3/\text{MeOH}$ 95:5 v/v) to yield **2** as an orange solid (0.024 g, 19%). M.p. 213.6–216.4°C; ^1H NMR (CDCl_3 , 600 MHz): $\delta = 8.71$ (t, 2H, $J = 7.47$ Hz, H^2, H^3), 8.36 (d, 1H, $J = 8.1$ Hz, H^7), 8.09 (s, 1H, H^8), 7.89 (d, 1H, $J = 7.47$ Hz, H^4), 7.83 (tr, 1H, $J = 5.26$ Hz, H^6), 7.79 (d, 2H, $J = 8.7$ Hz, H^9), 6.79 (d, 2H, $J = 8.82$ Hz, H^{10}), 4.28 (q, 2H, $J = 7.12$ Hz, H^2), 3.74–3.68 (m, 24H, H^{11-16}), 1.36 ppm (t, 3H, $J = 7.12$ Hz, H^1); ^{13}C NMR (CDCl_3 , 150 MHz): $\delta = 163.68, 163.16, 149.13, 148.48, 138.59, 132.29, 130.82, 129.87, 129.29, 128.63, 127.31, 126.71, 123.93, 123.46, 123.19, 120.20, 117.23, 112.01, 71.04-70.93, 68.82, 51.50, 35.93, 13.47$ ppm; HRMS (^+ESI): m/z : calcd for $\text{C}_{34}\text{H}_{40}\text{N}_5\text{O}_7$: 630.2928; found: 630.2883.

9-4-[4-(1,4,7,10,13-Pentaoxa-16-azacyclooctadecan-16-yl)phenyl]-1H-1,2,3-triazol-1-yl]-methylanthracene (3): Compounds **16** and **22** were reacted according to the general CuAAC procedure. The crude product was purified by column chromatography (silica gel, $\text{CHCl}_3/\text{MeOH}$ 97:3 v/v) to give **3** as a yellow solid (0.029 g, 22%). ^1H NMR (CDCl_3 , 600 MHz): $\delta = 8.59$ (s, 1H, H^1), 8.36 (d, 2H, $J = 8.70$ Hz, H^2), 8.09 (d, 2H, $J = 8.2$ Hz, H^3), 7.74–7.44 (m, 6H, $J = 8.2$ Hz, $\text{H}^4, \text{H}^5, \text{H}^6, \text{H}^7, \text{H}^8$), 7.15 (s, 1H, H^9), 6.59 (d, 2H, $J = 8.65$ Hz, H^9), 6.55 (s, 2H, H^6) 3.72–3.49 ppm (m, 24H, H^{10-15}); ^{13}C NMR (CDCl_3 , 150 MHz): $\delta = 148.40, 147.78, 131.66, 131.06, 129.91, 129.58, 127.77, 126.87, 125.57, 124.18, 123.27, 118.37, 117.66, 111.70, 70.98, 70.94, 70.89, 70.84, 68.76, 51.39$ ppm; HRMS (^+ESI): m/z calcd for $\text{C}_{35}\text{H}_{41}\text{N}_4\text{O}_5$: 597.3070; found: 597.3120.

10-Cyano-9-[4-[4-(1,4,7,10,13-pentaoxa-16-azacyclooctadecan-16-yl)phenyl]-1H-1,2,3-triazol-1-yl]-methylanthracene (4): Compounds **16** and **23** were reacted according to the general CuAAC procedure. Crude **4** was purified by column chromatography (silica gel, $\text{CHCl}_3/\text{MeOH}$ 97:3 v/v) with subsequent recrystallization from $\text{CH}_2\text{Cl}_2/\text{petrol ether}$ (50–70°C) 1:1 v/v, to give yellow crystals (0.028 g, 20%). M.p. 199.5–203.9°C; ^1H NMR (CDCl_3 , 600 MHz): $\delta = 8.53$ (d, 2H, $J = 8.64$ Hz, H^1), 8.49 (d, 2H, $J = 8.76$ Hz, H^2), 7.77 (m, 2H, H^3), 7.72 (m, 2H, H^3), 7.45 (d, 2H, $J = 9.0$ Hz, H^7), 7.18 (s, 1H, H^6), 6.59 (d, 2H, $J = 8.8$ Hz, H^8), 6.57 (s, 2H, H^5), 3.65–3.56 ppm (m, 24H, H^{9-15}); ^{13}C NMR (CDCl_3 , 150 MHz): $\delta = 148.68, 147.83, 133.00, 130.78, 130.05, 128.94, 128.52, 126.77, 126.59, 124.02, 117.74, 117.34, 116.81, 111.57, 108.84, 70.85, 70.80, 70.75, 70.70, 68.59,$

51.22, 46.27 ppm; HRMS (^+ESI): m/z : calcd for $\text{C}_{36}\text{H}_{40}\text{N}_5\text{O}_5$: 622.3029; found: 622.3065.

10-Methyl-9-[4-[4-(1,4,7,10,13-pentaoxa-16-azacyclooctadecan-16-yl)phenyl]-1H-1,2,3-triazol-1-yl]-methylanthracene (5): Compounds **16** and **24** were reacted according to the general CuAAC procedure. The crude product was purified by column chromatography ($\text{CHCl}_3/\text{MeOH}$ 97:3 v/v) with subsequent recrystallization from $\text{CH}_2\text{Cl}_2/\text{hexane/ethyl acetate}$ 1:1:0.25 v/v/v, to give **5** in form of brownish crystals (64 mg, 48%). M.p. 148.7–151.3°C; ^1H NMR (CDCl_3 , 500 MHz): $\delta = 8.41$ (dd, 2H, $J = 7.65, 0.60$ Hz, H^2), 8.41–8.31 (m, 2H, H^5), 7.61–7.56 (m, 4H, H^3, H^4), 7.44 (d, 2H, $J = 8.9$ Hz, H^8), 7.11 (s, 1H, H^7), 6.57 (d, 2H, $J = 8.9$ Hz, H^3), 6.55 (s, 2H, H^6), 3.66–3.56 (m, 24H, H^{10-15}), 3.19 ppm (s, 3H, H^1); ^{13}C NMR (CDCl_3 , 125 MHz): $\delta = 148.29, 147.73, 133.90, 130.73, 130.14, 127.22, 126.84, 126.15, 125.89, 125.44, 123.88, 122.50, 118.39, 117.71, 111.67, 70.97, 70.92, 70.87, 70.82, 68.74, 51.35, 46.79, 14.78$ ppm; HRMS (^+ESI): m/z calcd for $\text{C}_{36}\text{H}_{43}\text{N}_4\text{O}_5$: 611.3233; found: 611.3279.

4,4-Difluoro-8-[4-[1-[4-(1,4,7,10,13-pentaoxa-16-azacyclooctadecan-16-yl)phenyl]-1H-1,2,3-triazol-4-yl]phenyl]-1,3,7,9-tetramethyl-4-bora-3a,4a-diaza-s-indacene (6): Compounds **17** and **25** were reacted according to the general CuAAC procedure. Crude **6** was purified by column chromatography (silica gel, $\text{CHCl}_3/\text{MeOH/hexane}$ 80:7:13 v/v/v) to give **6** in the form of reddish crystals (0.040 g, 28%). M.p. 197.2199.4°C; ^1H NMR (CDCl_3 , 600 MHz): $\delta = 8.14$ (s, 1H, H^6), 8.04 (d, 2H, $J = 8.3$ Hz, H^5), 7.56 (d, 2H, $J = 8.9$ Hz, H^7), 7.38 (d, 2H, $J = 8.3$ Hz, H^4), 6.79 (d, 2H, $J = 8.9$ Hz, H^8), 5.99 (s, 2H, H^3), 3.75 (t, 4H, $J = 5.5$ Hz, H^9), 1.70–3.76 (m, 20H, H^{10-14}), 2.57 (s, 6H, H^2), 1.46 ppm (s, 6H, H^1); ^{13}C NMR (CDCl_3 , 150 MHz): $\delta = 155.72, 147.24, 143.27, 141.41, 134.90, 131.54, 128.77, 126.52, 122.36, 121.42, 118.28, 111.99, 71.02, 70.97, 70.93, 68.65, 51.63, 29.85, 14.79$ ppm; ^{19}F NMR (CDCl_3 , 300 MHz): $\delta = -146.7$ ppm (m, 2F); HRMS (^+ESI): m/z calcd for $\text{C}_{39}\text{H}_{48}\text{BF}_2\text{N}_6\text{O}_5$: 729.3747; found: 729.3746.

9-[1-[4-(1,4,7,10,13-Pentaoxa-16-azacyclooctadecan-16-yl)phenyl]-1H-1,2,3-triazol-4-yl]-anthracene (7): Compounds **17** and **18** were reacted according to the general CuAAC procedure. The crude product was purified by column chromatography (65 × 2 cm, silica gel, $\text{CHCl}_3/\text{MeOH}$ 95:5 v/v) to yield **7** as a light brown oil (0.021 g, 23%). ^1H NMR (CDCl_3 , 300 MHz): $\delta = 8.56$ (s, 1H, H^1), 8.11 (s, 1H, H^2), 8.10–8.00 (m, 2H, H^3), 7.99–7.93 (m, 2H, H^5), 7.55–7.40 (m, 4H, H^3, H^4), 6.87 (d, 2H, $J = 9.12$ Hz, H^7), 6.67 (d, 2H, $J = 9.12$ Hz, H^2), 3.73–3.59 ppm (m, 24H, H^{10-14}); ^{13}C NMR (CDCl_3 , 75 MHz): $\delta = 145.62, 148.02, 131.34, 131.02, 128.64, 126.89, 126.07, 124.54, 125.48, 125.21, 122.07, 119.95, 111.24, 70.85, 68.37, 51.16$ ppm; MS (^+ESI): m/z calcd for $\text{C}_{34}\text{H}_{39}\text{N}_4\text{O}_5$: 583.29; found: 583.34.

2-Ethyl-6-(4-octyl-1H-1,2,3-triazol-1-yl)-1H-benzo[de]isoquinoline-1,3(2H)-dione (9): 1-Decyne (0.021 g, 0.015) and **21** (0.04 g, 0.15 mmol) were reacted according to the general CuAAC procedure. The crude product was purified by column chromatography (silica gel, $\text{CHCl}_3/\text{MeOH}$ 250:1 v/v) to give **9** as an orange semi-solid (38 mg, 63%). ^1H NMR (CDCl_3 , 600 MHz): $\delta = 8.68$ (d, 2H, $J = 7.44$ Hz, H^9, H^2), 8.27 (d, 1H, $J = 8.58$ Hz, H^7), 7.83–7.80 (m, 2H, H^8, H^6), 7.78 (s, 1H, H^{10}), 4.26 (q, 2H, $J = 7.08$ Hz, H^2), 2.8 8(t, 2H, $J = 7.77$ Hz, H^{11}), 1.80 (qu, 2H, H^{12}), 1.30 (m, 2H, H^{13}), 1.39–1.24 (m, 11H, $\text{H}^1, \text{H}^{14-18}$), 0.88 ppm (t, 3H, $J = 7.0$ Hz, H^{18}); ^{13}C NMR (CDCl_3 , 150 MHz): $\delta = 163.63, 163.12, 149.41, 138.62, 132.24, 130.77, 129.76, 129.22, 128.58, 126.66, 123.87, 123.16, 123.14, 35.90, 31.99, 29.50, 29.47, 29.37, 25.78, 22.80, 14.24, 13.44$ ppm; MS (EI): m/z (%): 404 (100) [M^+].

1-1-[4-(1,4,7,10,13-Pentaoxa-16-azacyclooctadecan-16-yl)phenyl]-1H-1,2,3-triazol-4-yl]-octan (10): Compound **17** (0.05 g, 0.13 mmol) and 1-decyne (0.018 g, 0.13 mmol) were dissolved in THF/water (3:1 v/v, 4 mL) and CuSO_4 (1.7 mg, 0.007 mmol, 5 mol %) and sodium ascorbate (2.6 mg, 0.013 mmol, 10 mol %) were added.^[66] The reaction mixture was stirred at 60°C for 16 h. Aqueous NH_4Cl (10%, 4 mL) was added and the THF was removed under reduced pressure. The aqueous layer was extracted with dichloromethane (3 × 7 mL), the organic layer was dried with MgSO_4 and concentrated. The crude product was purified by column chromatography (silica gel, ethyl acetate/MeOH 7:3) to give **10** as a greenish oil (0.072 g, >99%). ^1H NMR (CDCl_3 , 300 MHz): $\delta = 7.56$ (s, 1H, H^9), 7.58 (d, 2H, $J = 9.04$ Hz, H^{10}), 6.76 (d, 2H, $J = 7.35$ Hz, H^{11}), 3.74–3.66 (m, 24H, H^{12-17}), 2.76 (tr, 2H, $J = 7.53$ Hz, H^8), 1.71 (qu, 2H, $J = 7.72$ Hz, H^7), 1.41–1.22 (m, 10H, H^{2-6}), 0.87 ppm (tr, 3H, $J = 6.97$ Hz,

H¹); ¹³C NMR (CDCl₃, 75 MHz): δ = 149.09, 122.44 (3×), 119.24, 112.79, 70.82–70.74, 68.86, 52.26, 32.24, 29.86, 29.74, 29.68, 29.59, 26.11, 23.03, 14.44 ppm; HRMS (EI): *m/z* calcd for C₂₈H₄₇N₄O₅: 518.3546; found: 518.3545.

9-[4-(Octyl)-1H-1,2,3-triazol-1-yl]-methylanthracene (12): The reaction followed the procedure outlined for **10** using **22** (0.07 g, 0.3 mmol) and 1-decyne (0.041 g, 0.3 mmol). The crude product was purified by column chromatography (silica gel, ethyl acetate/hexane 1:1) to give **12** as a yellow solid (0.081 g, 72%). M.p. 113°C, ¹H NMR (CDCl₃, 300 MHz): δ = 8.58 (s, 1H, H¹⁵), 8.33 (d, 2H, *J* = 8.10 Hz, H¹⁴), 8.08 (d, 2H, *J* = 8.30 Hz, H¹¹), 7.60–7.50 (m, 4H, H¹², H¹³), 6.82 (s, 1H, H⁹), 6.50 (s, 2H, H¹⁰), 2.51 (t, 2H, *J* = 7.72 Hz, H⁸), 1.48 (qu, 2H, *J* = 7.72 Hz, H⁷), 1.26–1.17 (m, 10H, H^{2–6}), 0.83 ppm (t, 3H, *J* = 6.59 Hz, H¹); ¹³C NMR (CDCl₃, 75 MHz): δ = 138.55, 137.60, 131.53, 130.91, 129.68, 129.43, 128.09, 127.55, 125.39, 124.20, 123.77, 123.144, 120.93, 119.99, 48.72, 46.33, 31.75, 29.29, 29.17, 29.09, 25.68, 22.57, 13.99 ppm; HRMS (EI): *m/z* calcd for C₂₅H₃₀N₃: 372.2440; found: 372.2442.

9-[1-(Octyl)-1H-1,2,3-triazol-4-yl]-anthracene (15): Compound **18** (0.169 g, 0.084 mmol) and **19** (0.13 g, 0.084 mmol) were reacted according to the general CuAAC procedure. The crude product was purified by column chromatography (silica gel, CHCl₃) to give **15** as a dark orange oil (0.106 g, 35%). ¹H NMR (CDCl₃, 600 MHz): δ = 8.53 (s, 1H, H¹), 8.04 (dd, 2H, *J* = 8.07, 0.69 Hz, H²), 7.82 (dd, 2H, *J* = 7.92, 0.96 Hz, H²), 7.76 (s, 1H, H⁶), 7.46 (m, 2H, H³), 7.40 (m, 2H, H³), 4.57 (t, 2H, *J* = 7.23 Hz, H⁷), 2.09 (qu, 2H, *J* = 7.35 Hz, H⁸), 1.5–1.3 (m, 10H, H), 0.90 ppm (t, 3H, *J* = 6.96 Hz, H¹⁴); ¹³C NMR (CDCl₃, 150 MHz): δ = 144.04, 131.45, 128.61, 128.35, 126.16, 125.36, 124.661, 50.78, 31.85, 30.59, 29.27, 29.15, 26.79, 22.77, 14.24 ppm; MS (+ESI): *m/z*: calcd for: 358.23; found: 358.38; MS (EI): *m/z* (%): 357(100) [M⁺].

Acknowledgements

Financial support from the DFG GRK 837 is gratefully acknowledged. We thank Roman Flehr for time-resolved fluorescence measurements of compounds **3–5** and Dr. S. Czaplá for providing the Cu/C catalyst for the “click” reactions.

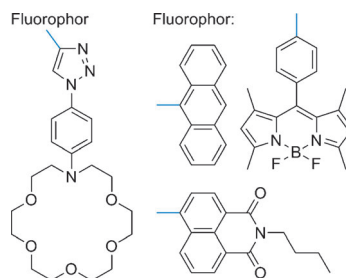
- A. G. O'Donnell, I. M. Young, S. P. Rushton, M. D. Shirley, J. W. Crawford, *Nat. Rev. Microbiol.* **2007**, *5*, 689–699.
- L. Chaerle, S. Lenk, I. Leinonen, H. G. Jones, D. Van Der Straeten, C. Buschmann, *Biotechnol. J.* **2009**, *4*, 1152–1167.
- W. Wang, M. W. Vaughn, *Scanning* **2008**, *30*, 65–77.
- T. E. Hébert, C. Gales, R. V. Rebois, *Cell Biochem. Biophys.* **2006**, *45*, 85–109.
- J. W. Borst, A. J. W. G. Visser, *Meas. Sci. Technol.* **2010**, *21*, 102002.
- L. D. Lavis, *J. Histochem. Cytochem.* **2011**, *59*, 139–145.
- R. L. Nicholson, M. Welch, M. Ladlow, D. R. Spring, *ACS Chem. Biol.* **2007**, *2*, 24–30.
- L. Evensen, W. Link, J. B. Lorens, *Curr. Pharm. Des.* **2010**, *16*, 3958–3963.
- M. I. J. Stich, L. H. Fischer, O. S. Wolfbeis, *Chem. Soc. Rev.* **2010**, *39*, 3102–3114.
- C. Charlton, V. Gubala, R. P. Gandhiraman, J. Wiechecki, N. C. H. Le, C. Coyle, S. Daniels, B. D. MacCraith, D. E. Williams, *J. Colloid Interface Sci.* **2011**, *354*, 405–409.
- S. M. Borisov, O. S. Wolfbeis, *Chem. Rev.* **2008**, *108*, 423–461.
- R. Y. Tsien, *Angew. Chem.* **2009**, *121*, 5721–5736; *Angew. Chem. Int. Ed.* **2009**, *48*, 5612–5626.
- T. Klingstedt, K. P. R. Nilsson, *Biochim. Biophys. Acta Gen. Subj.* **2011**, *1810*, 286–296.
- K. E. Sapsford, L. Berti, I. L. Medintz, *Minerva Biotechnologica* **2004**, *16*, 247–273.
- Y. Yan, M. E. Marriott, C. Petchprayoon, G. Marriott, *Biochem. J.* **2011**, *433*, 411–422.
- I. L. Medintz, H. T. Uyeda, E. R. Goldman, H. Mattoussi, *Nat. Mater.* **2005**, *4*, 435–446.
- D. K. Chatterjee, M. K. Gnanasammandhan, Y. Zhang, *Small* **2010**, *6*, 2781–2795.
- W. P. Heal, T. H. Tam Dang, E. W. Tate, *Chem. Soc. Rev.* **2011**, *40*, 246–257.
- J. Wu, W. Liu, J. Ge, H. Zhang, P. Wang, *Chem. Soc. Rev.* **2011**, *40*, 3483–3495.
- A. P. de Silva, T. S. Moody, G. D. Wright, *Analyst* **2009**, *134*, 2385–2393.
- B. Valeur, I. Leray, *Coord. Chem. Rev.* **2000**, *205*, 3–40.
- A. P. de Silva, H. Q. Nimal Gunaratne, T. Gunnlaugsson, A. J. M. Huxley, C. P. McCoy, J. T. Rademacher, T. E. Rice, *Chem. Rev.* **1997**, *97*, 1515–1566.
- Still today, some of the early ICT probes for alkali and alkaline-earth metal ions developed by Tsien's group show unrivalled performance in realistic environments. However, it should be noted that these probes only show pronounced fluorescence excitation spectral shifts, yet weak fluorescence intensity changes.^[24,25] In the case of K⁺, these effects are still even poorer as has been shown by Sammes' as well as Kurtz's groups.^[26–28]
- A. Minta, R. Y. Tsien, *J. Biol. Chem.* **1989**, *264*, 19449–19457.
- G. Grynkiewicz, M. Poenie, R. Y. Tsien, *J. Biol. Chem.* **1985**, *260*, 3440–3450.
- R. Crossley, Z. Goolamali, J. J. Gosper, P. G. Sammes, *J. Chem. Soc. Perkin Trans. 2* **1994**, 513–520.
- R. Crossley, Z. Goolamali, P. G. Sammes, *J. Chem. Soc. Perkin Trans. 2* **1994**, 1615–1623.
- K. Golchini, M. Mackovic-Basic, S. A. Gharib, D. Masilamani, M. E. Lucas, I. Kurtz, *Am. J. Physiol.* **1990**, *258*, F438–F443.
- Although some of these systems show favorable fluorescence enhancement factors in actual applications.^[30,31]
- M. Shortreed, R. Kopelman, M. Kuhn, B. Hoyland, *Anal. Chem.* **1996**, *68*, 1414–1418.
- H. He, M. A. Mortellaro, M. J. P. Leiner, R. J. Fraatz, J. K. Tusa, *J. Am. Chem. Soc.* **2003**, *125*, 1468–1469.
- Advanced Fluorescence Reporters in Chemistry and Biology I: Fundamentals and Molecular Design, Series on Fluorescence, Vol. 8* (Ed.: A. P. Demchenko), Springer, **2010**.
- Advanced Fluorescence Reporters in Chemistry and Biology II: Molecular Constructions, Polymers and Nanoparticles, Series on Fluorescence, Vol. 9* (Ed.: A. P. Demchenko), Springer, Berlin, **2010**.
- K. J. Wallace, *Supramol. Chem.* **2009**, *21*, 89–102.
- Z. Qin, J. A. Caruso, B. Lai, A. Matusch, J. S. Becker, *Metallomics* **2011**, *3*, 28–37.
- O. Gerasimenko, A. Tepikin, *Cell Calcium* **2005**, *38*, 201–211.
- R. B. Thompson, *Curr. Opin. Chem. Biol.* **2005**, *9*, 526–532.
- N. V. Pechishcheva, K. Y. Shunyaev, *J. Anal. Chem.* **2008**, *63*, 412–423.
- B. Chen, J. Liang, X. Tian, X. Liu, *Biochemistry (Moscow)* **2008**, *73*, 853–861.
- J. F. Zhang, Y. Zhou, J. Yoon, J. S. Kim, *Chem. Soc. Rev.* **2011**, *40*, 3416–3429.
- D.-L. Ma, D. S.-H. Chan, B. Y.-W. Man, C.-H. Leung, *Chem. Asian J.* **2011**, *6*, 986–1003.
- S. Sumalekshmy, C. J. Fahrni, *Chem. Mater.* **2011**, *23*, 483–500.
- H. M. Kim, B. R. Cho, *Chem. Asian J.* **2011**, *6*, 58–69.
- “Hard” in terms of Pearson's concept of “hard and soft acids and bases” (HSAB), see refs. [45,46].
- R. G. Pearson, *J. Am. Chem. Soc.* **1963**, *85*, 3533–3539.
- R. G. Pearson, *Inorg. Chem.* **1988**, *27*, 734–740.
- M. Kollmannsberger, K. Rurack, U. Resch-Genger, J. Daub, *J. Phys. Chem. A* **1998**, *102*, 10211–10220.
- M. Kollmannsberger, K. Rurack, U. Resch-Genger, W. Rettig, J. Daub, *Chem. Phys. Lett.* **2000**, *329*, 363–369.
- J.-P. Malval, I. Leray, B. Valeur, *New J. Chem.* **2005**, *29*, 1089–1094.
- M. Baruah, W. Qin, R. A. L. Valle, D. Beljonne, T. Rohand, W. Dehaen, N. Boens, *Org. Lett.* **2005**, *7*, 4377–4380.

- [51] I. Móczár, P. Huszthy, Z. Maidics, M. Kadar, K. Toth, *Tetrahedron* **2009**, *65*, 8250–8258.
- [52] Z. Shen, H. Röhr, K. Rurack, H. Uno, M. Spieles, B. Schulz, G. Reck, N. Ono, *Chem. Eur. J.* **2004**, *10*, 4853–4871.
- [53] A. B. Descalzo, S. Zhu, T. Fischer, K. Rurack, in *Advanced Fluorescence Reporters in Chemistry and Biology II, Series on Fluorescence, Vol. 9* (Ed.: A. P. Demchenko), Springer, Berlin, **2010**, pp. 41–106.
- [54] K. Rurack, M. Kollmannsberger, U. Resch-Genger, J. Daub, *J. Am. Chem. Soc.* **2000**, *122*, 968–969.
- [55] T. Schwarze, H. Müller, C. Dosche, T. Klamroth, W. Mickler, A. Kelling, H.-G. Löhmansröben, P. Saalfrank, H.-J. Holdt, *Angew. Chem.* **2007**, *119*, 1701–1704; *Angew. Chem. Int. Ed.* **2007**, *46*, 1671–1674.
- [56] T. Schwarze, C. Dosche, R. Flehr, T. Klamroth, H.-G. Löhmansröben, P. Saalfrank, E. Cleve, H.-J. Buschmann, H.-J. Holdt, *Chem. Commun.* **2010**, *46*, 2034–2036.
- [57] S. Berndt, N. Herzig, P. Kele, D. Lachmann, X. Li, O. S. Wolfbeis, H.-A. Wagenknecht, *Bioconjugate Chem.* **2009**, *20*, 558–564.
- [58] M. V. Gil, M. J. Arévalo, Ó. López, *Synthesis* **2007**, 1589–1620.
- [59] S. Huang, R. J. Clark, L. Zhu, *Org. Lett.* **2007**, *9*, 4999–5002.
- [60] Y. H. Lau, P. J. Rutledge, M. Watkinson, M. H. Todd, *Chem. Soc. Rev.* **2011**, *40*, 2848–2866.
- [61] S. Y. Park, J. H. Yoon, C. S. Hong, R. Souane, J. S. Kim, S. E. Matthews, J. Vicens, *J. Org. Chem.* **2008**, *73*, 8212–8218.
- [62] E. Tamanini, A. Katewa, L. M. Sedger, M. H. Todd, M. Watkinson, *Inorg. Chem.* **2009**, *48*, 319–324.
- [63] D. Maity, T. Govindaraju, *Inorg. Chem.* **2010**, *49*, 7229–7231.
- [64] E. Hao, T. Meng, M. Zhang, W. Pang, Y. Zhou, L. Jiao, *J. Phys. Chem. A* **2011**, *115*, 8234–8241.
- [65] Y.-B. Ruan, S. Maisonneuve, J. Xie, *Dyes Pigm.* **2011**, *90*, 239–244.
- [66] S. Maisonneuve, Q. Fang, J. Xie, *Tetrahedron* **2008**, *64*, 8716–8720.
- [67] X.-P. He, Z. Song, Z.-Z. Wang, X.-X. Shi, K. Chen, G.-R. Chen, *Tetrahedron* **2011**, *67*, 3343–3347.
- [68] H. A. Michaels, C. S. Murphy, R. J. Clark, M. W. Davidson, L. Zhu, *Inorg. Chem.* **2010**, *49*, 4278–4287.
- [69] K. Varazo, F. Xie, D. Gullledge, Q. Wang, *Tetrahedron Lett.* **2008**, *49*, 5293–5296.
- [70] P. D. Jarowski, Y.-L. Wu, W. B. Schweizer, F. Diederich, *Org. Lett.* **2008**, *10*, 3347–3350.
- [71] Our approach employing a coumarin dye has recently been published in a separate paper.^[72]
- [72] S. Ast, H. Müller, R. Flehr, T. Klamroth, B. Walz, H.-J. Holdt, *Chem. Commun.* **2011**, *47*, 4685–4687.
- [73] V. Souchon, S. Maisonneuve, O. David, I. Leray, J. Xie, B. Valeur, *Photochem. Photobiol. Sci.* **2008**, *7*, 1323–1331.
- [74] E. Tamanini, K. Flavin, M. Motevalli, S. Piperno, L. A. Gheber, M. H. Todd, M. Watkinson, *Inorg. Chem.* **2010**, *49*, 3789–3800.
- [75] K. Jobe, C. H. Brennan, M. Motevalli, S. M. Goldup, M. Watkinson, *Chem. Commun.* **2011**, *47*, 6036–6038.
- [76] LE state = locally excited state, that is, a fluorescence arising from an excited state that is exclusively located on a certain fluorophore fragment, see also discussion in the section regarding **7**.
- [77] J. W. Sibert, P. B. Forshee, *Inorg. Chem.* **2002**, *41*, 5928–5930.
- [78] J. W. Sibert, P. B. Forshee, G. R. Hundt, A. L. Sargent, S. G. Bott, V. Lynch, *Inorg. Chem.* **2007**, *46*, 10913–10925.
- [79] H. Guo, M. L. Muro-Small, S. Ji, J. Zhao, F. N. Castellano, *Inorg. Chem.* **2010**, *49*, 6802–6804.
- [80] Z. Li, R. Bittman, *J. Org. Chem.* **2007**, *72*, 8376–8382.
- [81] C. Tahtaoui, C. Thomas, F. Rohmer, P. Klotz, G. Duportail, Y. Mély, D. Bonnet, M. Hibert, *J. Org. Chem.* **2007**, *72*, 269–272.
- [82] D.-N. Lee, G.-J. Kim, H.-J. Kim, *Tetrahedron Lett.* **2009**, *50*, 4766–4768.
- [83] J. Li, M. Hu, S. Q. Yao, *Org. Lett.* **2009**, *11*, 3008–3011.
- [84] Q. Xiao, R. T. Ranasinghe, A. M. P. Tang, T. Brown, *Tetrahedron* **2007**, *63*, 3483–3490.
- [85] J. D. Lewis, J. N. Moore, *Dalton Trans.* **2004**, 1376–1385.
- [86] K.-C. Chang, I.-H. Su, A. Senthilvelan, W.-S. Chung, *Org. Lett.* **2007**, *9*, 3363–3366.
- [87] A. Torrado, B. Imperiali, *J. Org. Chem.* **1996**, *61*, 8940–8948.
- [88] R. Liu, M. A. Winnik, F. Di Stefano, J. Vanketessan, *J. Polym. Sci. Part A* **2001**, *39*, 1495–1504.
- [89] S. Saha, A. Samanta, *J. Phys. Chem. A* **2002**, *106*, 4763–4771.
- [90] Note that the different nature of an alkyl substituent at the imide nitrogen of the naphthalimide unit, for example, *n*-butyl and ethyl, has virtually no influence on the photophysics, see ref. [91].
- [91] M. S. Alexiou, V. Tychoopoulos, S. Ghorbanian, J. H. P. Tyman, R. G. Brown, P. I. Brittain, *J. Chem. Soc. Perkin Trans. 2* **1990**, 837–842.
- [92] The feasibility of using the dimethylamino instead of the aza crown compound in quantum chemical calculations to save computing time has been demonstrated, see ref. [93].
- [93] W. Rettig, K. Rurack, M. Sczepan in *New Trends in Fluorescence Spectroscopy. Applications to Chemical and Life Sciences, Series on Fluorescence, Vol. 1* (Eds.: B. Valeur, J. C. Brochon), Springer, Berlin, **2001**, pp. 125–155.
- [94] K. Rurack, M. Sczepan, M. Spieles, U. Resch-Genger, W. Rettig, *Chem. Phys. Lett.* **2000**, *320*, 87–94.
- [95] Recently, Katan and co-workers also confirmed such behaviour and showed that a change from TD-DFT to, for instance, a more Fock-like orbital exchange treatment can account for this problem yet has other trade-offs.^[96] We thus used the method which allows comparison with Diederich's data.
- [96] C. Katan, M. Blanchard-Desce, S. Tretiak, *J. Chem. Theory Comput.* **2010**, *6*, 3410–3426.
- [97] S. Delmond, J.-F. Létard, R. Lapouyade, W. Rettig, *J. Photochem. Photobiol. A* **1997**, *105*, 135–148.
- [98] E. Lager, J. Liu, A. Aguilar-Aguilar, B. Z. Tang, E. Peña-Cabrera, *J. Org. Chem.* **2009**, *74*, 2053–2058.
- [99] B. Ramachandram, G. Saroja, B. Sankaran, A. Samanta, *J. Phys. Chem. B* **2000**, *104*, 11824–11832.
- [100] M. M. Martin, P. Plaza, N. D. Hung, Y. H. Meyer, J. Bourson, B. Valeur, *Chem. Phys. Lett.* **1993**, *202*, 425–430.
- [101] R. Mathevet, G. Jonusauskas, C. Rulliere, J.-F. Letard, R. Lapouyade, *J. Phys. Chem.* **1995**, *99*, 15709–15713.
- [102] K. Rurack, J. L. Bricks, G. Reck, R. Radeaglia, U. Resch-Genger, *J. Phys. Chem. A* **2000**, *104*, 3087–3109.
- [103] H.-J. Buschmann in *Stereochemical and Stereophysical Behaviour of Macrocycles* (Ed.: I. Bernal), Elsevier, Amsterdam, **1987**, pp. 103–185.
- [104] A. Masuyama, Y. Nakatsuji, I. Ikeda, M. Okahara, *Tetrahedron Lett.* **1981**, *22*, 4665–4668.
- [105] D. Yuan, R. G. Brown, *J. Phys. Chem. A* **1997**, *101*, 3461–3466.
- [106] S. Dhar, S. S. Roy, D. K. Rana, S. Bhattacharya, S. Bhattacharya, S. C. Bhattacharya, *J. Phys. Chem. A* **2011**, *115*, 2216–2224.
- [107] A. P. de Silva, H. Q. N. Gunaratne, G. E. M. Maguire, *J. Chem. Soc. Chem. Commun.* **1994**, 1213–1214.
- [108] T. Gunnlaugsson, M. Nieuwenhuysen, L. Richard, V. Thoss, *J. Chem. Soc. Perkin Trans. 2* **2002**, 141–150.
- [109] C. S. Park, J. Y. Lee, E.-J. Kang, J. E. Lee, S. S. Lee, *Tetrahedron Lett.* **2009**, *50*, 671–675.
- [110] A. P. de Silva, H. Q. N. Gunaratne, K. R. A. S. Sandanayake, *Tetrahedron Lett.* **1990**, *31*, 5193–5196.
- [111] –2170 mV (for anthracene), –2190 mV (for 9-methylanthracene) and –1360 mV (for 9-cyanoanthracene) have been determined in the literature, see ref. [114]. In addition, we have determined the respective reduction potentials here to –2020 mV for 9,10-dimethylanthracene and –1480 mV for 9-cyano-10-methylanthracene. The corresponding oxidation potentials reported by Okazaki et al.^[114] amount to +1100 mV (for anthracene), +990 mV (for 9-methylanthracene) and +1390 mV (for 9-cyanoanthracene) as well as +1070 mV for 9,10-dimethylanthracene and +1480 mV for 9-cyano-10-methylanthracene as obtained by us in this study.
- [112] The oxidation at +1470 mV in **12** is attributed to the isolated triazole moiety, since it is absent in anthracene and 9-methylanthracene.
- [113] ΔG [eV] = $E(D^+/D) - E(A/A^-) - E_{00} - 0.06$ eV, the latter being the charge separation term in MeCN, cf. ref. [115], ΔG = PET driving

- force; $E(D^+/D)$, $E(A/A^-)$ =oxidation and reduction potentials of donor and acceptor moiety; E_{00} =energy of 0–0 electronic transition.
- [114] S. Okazaki, M. Oyama, S. Nomura, *Electroanalysis* **1997**, *9*, 1242–1246.
- [115] J. R. Lakowicz, *Principles of Fluorescence Spectroscopy*, Springer, New York, 3rd ed., **2006**, p. 337.
- [116] G. Ulrich, R. Ziessel, A. Harriman, *Angew. Chem.* **2008**, *120*, 1202–1219; *Angew. Chem. Int. Ed.* **2008**, *47*, 1184–1201.
- [117] A. Loudet, K. Burgess, *Chem. Rev.* **2007**, *107*, 4891–4932
- [118] K. Rurack, U. Resch-Genger, *Chem. Soc. Rev.* **2002**, *31*, 116–127.
- [119] N. Boens, V. Leen, W. Dehaen, *Chem. Soc. Rev.* **2012**, *41*, 1130–1172.
- [120] R. Hu, E. Lager, A. Aguilar-Aguilar, J. Liu, J. W. Y. Lam, H. H. Y. Sung, I. D. Williams, Y. Zhong, K. S. Wong, E. Peña-Cabrera, B. Z. Tang, *J. Phys. Chem. C* **2009**, *113*, 15845–15853.
- [121] M. Bhuyan, E. Katayev, S. Stadlbauer, H. Nonaka, A. Ojida, I. Hamachi, B. König, *Eur. J. Org. Chem.* **2011**, 2807–2817.
- [122] H. Shizuka, T. Ogiwara, E. Kimura, *J. Phys. Chem.* **1985**, *89*, 4302–4306.
- [123] The angles describe the twisting angles between the planes of the two mono- and the trinuclear ring systems with all the respective ring atoms defining the planes. The angle between phenyl and anthryl unit equals 85.0°.
- [124] Between S_6 and S_{17} , only considerably weak (mixed) transitions with $f < 0.06$ and no pronounced CT character are found. $S_{17} \leftarrow S_0$ at 238.9 nm then is the oscillator-strongest transition ($f = 1.052$) and basically distributed on anthracene-localized MOs. This transition can be assigned to the intense band at 254 nm in the absorption spectrum of **7** in Figure 7, originating mainly from anthracene. For details, see Figure S5 and Table S8.
- [125] W. Rettig, R. Lapouyade, in *Probe Design and Chemical Sensing*, Topics in Fluorescence Spectroscopy (Ed.: J. R. Lakowicz), Plenum Press, New York, **1994**, pp. 109–149.
- [126] M. A. Haidekker, M. Nipper, A. Mustafic, D. Lichlyter, M. Dakanali, E. A. Theodorakis, in *Advanced Fluorescence Reporters in Chemistry and Biology I, Series on Fluorescence, Vol. 8* (Ed.: A. P. Demchenko), Springer, Berlin, **2010**, pp. 267–308.
- [127] Less decoupled probes have only rarely been described and required aprotic or protic organic solvents for operation, see refs. [128, 129].
- [128] S. A. Jonker, S. I. Van Dijk, K. Goubitz, C. A. Reiss, W. Schuddeboom, J. W. Verhoeven, *Molecular Crystals and Liquid Crystals* **1990**, *183*, 273–282.
- [129] K. Rurack, M. Kollmannsberger, J. Daub, *New J. Chem.* **2001**, *25*, 289–292.
- [130] S. Fery-Forgues, M. T. Le Bris, J. P. Guette, B. Valeur, *J. Phys. Chem.* **1988**, *92*, 6233–6237.
- [131] For ICT-ICT systems, see refs. [132, 133] For ICT-PET systems, see refs. [134, 135].
- [132] K. Rurack, W. Rettig, U. Resch-Genger, *Chem. Commun.* **2000**, 407–408.
- [133] K. Rurack, A. Koval'chuck, J. L. Bricks, J. L. Slominskii, *J. Am. Chem. Soc.* **2001**, *123*, 6205–6206.
- [134] K. Rurack, J. L. Bricks, B. Schulz, M. Maus, G. Reck, U. Resch-Genger, *J. Phys. Chem. A* **2000**, *104*, 6171–6188.
- [135] K. Rurack, C. Trieflinger, A. Koval'chuck, J. Daub, *Chem. Eur. J.* **2007**, *13*, 8998–9003.
- [136] C. A. Parker, W. T. Rees, *Analyst* **1960**, *85*, 587–600.
- [137] R. A. Velapoldi, K. D. Mielenz, *A Fluorescence Standard Reference Material: Quinine Sulfate Dihydrate*, National Bureau of Standards special publication. Department of Commerce, National Bureau of Standards, **1980**.
- [138] K. Rurack, M. Spieles, *Anal. Chem.* **2011**, *83*, 1232–1242.
- [139] U. Resch-Genger, K. Rurack, *Proc. SPIE-Int. Soc. Opt. Eng.* **1997**, *3105*, 96–103.
- [140] Gaussian03 (Revision D.01), M. J. Frisch, G. W. Trucks, H. B. Schlegel, G. E. Scuseria, M. A. Robb, J. R. Cheeseman, J. A. Montgomery Jr., T. Vreven, K. N. Kudin, J. C. Burant, J. M. Millam, S. S. Iyengar, J. Tomasi, V. Barone, B. Mennucci, M. Cossi, G. Scalmani, N. Rega, G. A. Petersson, H. Nakatsuji, M. Hada, M. Ehara, K. Toyota, R. Fukuda, J. Hasegawa, M. Ishida, T. Nakajima, Y. Honda, O. Kitao, H. Nakai, M. Klene, X. Li, J. E. Knox, H. P. Hratchian, J. B. Cross, C. Adamo, J. Jaramillo, R. Gomperts, R. E. Stratmann, O. Yazyev, A. J. Austin, R. Cammi, C. Pomelli, J. W. Ochterski, P. Y. Ayala, K. Morokuma, G. A. Voth, P. Salvador, J. J. Dannenberg, V. G. Zakrzewski, S. Dapprich, A. D. Daniels, M. C. Strain, O. Farkas, D. K. Malick, A. D. Rabuck, K. Raghavachari, J. B. Foresman, J. V. Ortiz, Q. Cui, A. G. Baboul, S. Clifford, J. Ciołowski, B. B. Stefanov, G. Liu, A. Liashenko, P. Piskorz, I. Komaromi, R. L. Martin, D. J. Fox, T. Keith, M. A. Al-Laham, C. Y. Peng, A. Nanayakkara, M. Challacombe, P. M. W. Gill, B. Johnson, W. Chen, M. W. Wong, C. Gonzalez, J. A. Pople, Gaussian, Inc., Wallingford CT, **2004**.
- [141] D. Jiménez, R. Martínez-Máñez, F. Sancenón, J. V. Ros-Lis, J. Soto, Á. Benito, E. García-Breijo, *Eur. J. Inorg. Chem.* **2005**, 2393–2403.
- [142] S. G. Álvarez, M. T. Álvarez, *Synthesis* **1997**, 413–414.
- [143] L. S. Campbell-Verduyn, L. Mirfeizi, R. A. Dierckx, P. H. Elsinga, B. L. Feringa, *Chem. Commun.* **2009**, 2139–2141.
- [144] T. Gunnlaugsson, P. E. Kruger, P. Jensen, J. Tierney, H. D. P. Ali, G. M. Hussey, *J. Org. Chem.* **2005**, *70*, 10875–10878.
- [145] B. H. Lipshutz, B. R. Taft, *Angew. Chem.* **2006**, *118*, 8415–8418; *Angew. Chem. Int. Ed.* **2006**, *45*, 8235–8238.

Received: May 6, 2012
Published online: ■ ■ ■, 0000

Light-Up: Combination of a typical alkali metal ion receptor with various popular fluorophores in different signalling architectures through simple clicking of the modular precursors yields probes that integrate a novel donor-acceptor-substituted 1,2,3-triazole motif which gives rise to interesting absorption and fluorescence responses upon target binding.



Fluorescent Probes

*S. Ast, T. Fischer, H. Müller,
W. Mickler, M. Schwichtenberg,
K. Rurack,* H.-J. Holdt** ■■■-■■■

**Integration of the 1,2,3-Triazole
“Click” Motif as a Potent Signalling
Element in Metal Ion Responsive
Fluorescent Probes**

